Unterschrift des Betreuers

Diplomarbeit

Erosion analysis of thin W layers and W Fuzz under Ar ion bombardment

Ausgeführt am Institut für
Angewandte Physik
der Technischen Universität Wien
Wiedner Hauptstraße 8-10 / 134
1040 Wien

unter der Anleitung von
Univ.Prof. Dr. **Friedrich AUMAYR**

und
Dipl.-Ing. Dr. **Reinhard STADLMAYR**

durch
Daniel MAYER BSc.
Matrikelnr.: 1325067
[redacted]

Wien, 14.12.2021 (Daniel Mayer)

1 Kurzfassung

Es scheint schier unvorstellbar mit welch rasanter technologischer Entwicklung die Menschheit voranschreitet. Im Jahre 1866 wurden durch die Entdeckung des dynamo-elektrischen Prinzips erstmals großflächige, öffentliche Energieversorgungen möglich und heute stehen wir kurz davor, winzige Sonnen mittels Kernfusion kontrolliert entstehen zu lassen, um unseren nie enden wollenden Energiebedarf weiterhin decken zu können. Das junge Teilgebiet der Physik, die Plasmaphysik, bildet die Grundlage für das Verständnis rund um die Zusammenhänge eines quasineutralen Gases, genannt Plasma. Die vielversprechenste Möglichkeit, um eine Kernfusion von Wasserstoff zu Helium auf der Erde zu erzielen, besteht im magnetischen Einschluss eines D-T-Plasmas. Dieser Einschluss kann entweder durch einen TOKAMAK oder einen Stellarator realisiert werden, welche sich in der Erzeugung des erforderlichen poloidalen Magnetfeldes unterscheiden. Aus wirtschaftlicher und konstruktionstechnischer Sicht wurde der TOKAMAK Reaktor als geeigneter Kandidat für den Bau eines zukünftigen Kernfusionskraftwerk DEMO herangezogen, doch es warten noch große Herausforderungen.

Die für eine Fusion notwendigen physikalischen Bedingungen sind extrem und stellen speziell an die verwendeten Materialien der Innenwand des Reaktors unglaublich hohe Anforderungen. Die Erosionsrate ist hierbei ein maßgebliches und entscheidendes Kriterium für die Lebensdauer und somit für die Einsatzfähigkeit von Plasmarandschichtmaterialien. Aufgrund seiner bestechenden Eigenschaften, dem sehr hohen Schmelzpunkt, der geringen Tritium Rückhaltung und der äußerst niedrigen Zerstäubungsrate gilt Wolfram als hervorragende Wahl für die Diverterregion [1]. Jedoch wurde beobachtet, dass Wolfram unter gewissen Bedingungen eine fasrige Nanostruktur bildet, welche als W-Fuzz bezeichnet wird [2, 3]. Thermische sowie optische Eigenschaften werden durch diese Oberflächenveränderung negativ beeinflusst und man könnte vermuten, dass auch die Erosionsrate aufgrund der hochporösen Struktur erhöht ist [4, 5]. Im Zuge dieser Arbeit wurde das Erosionsverhalten von glatten W Proben und W-Fuzz Proben unter 2 keV Ar^{1+} Ionenbeschuss untersucht. Mit der bewährten und hochpräzisen TU Wien Quarzkristall-Mikrowaagen Technik (QCM) wurde unter Ultrahochvakuum (UHV) Bedingungen in-situ die Zerstäubungsrate der einzelnen W Probenoberflächen vermessen. Für die Untersuchung der W-Fuzz Probe wurde die QCM als Auffänger gegenüber der Probe installiert und mittels Kalibrierungsmessungen die Zerstäubungsrate errechnet. Erstaunlicherweise wurde für W-Fuzz eine deutlich niedrigere Zerstäubungsausbeute beobachtet als für glatte W-Proben. Dies lässt sich allerdings gut mit Redeposition des zerstäubten Wolframs in den fasrigen Strukturen des W-Fuzz erklären.

2 Abstract

It seems almost incredible to imagine the pace at which mankind is advancing in terms of technological development. The discovery of the dynamo-electric principle in 1866 made large-scale public energy supplies possible for the first time. Today, we are on the verge of creating our own tiny suns in reactors through nuclear fusion in order to keep satisfying our never-ending energy demand. Plasma physics is the fundamental basis for understanding the interactions of a quasineutral gas called plasma. On Earth the most promising way for achieving nuclear fusion of hydrogen to helium is by magnetic confinement of a D-T-plasma. This can be realized either by a TOKAMAK or a STELLERATOR, which differ in the way they generate the required poloidal magnetic field. From an economic and engineering point of view, the TOKAMAK reactor has been taken as the most suitable candidate for the construction of a future nuclear fusion power plant DEMO, but there are major challenges remaining.

The physical conditions necessary for fusion are extraordinary and cause enormous challenges especially for plasma-facing materials (PFM). In this regard, the erosion rate is a significant and decisive criterion for the inner wall's lifetime and thus for the usability of potential PFMs. Tungsten (W) is considered to be an excellent choice as PFM, especially for the diverter region due to its very high melting point, low tritium retention and extremely low sputtering yield [1]. However, it has been observed that under certain conditions, a tungsten surface forms fibrous nanostructures, called W-fuzz [2, 3]. Thermal and optical properties are negatively affected by this surface change and one could imagine that the erosion rate is also increased due to the weakened structure of this highly porous material [4, 5]. In the course of this diploma thesis, the erosion behavior of smooth W samples and W fuzz samples under 2 keV Ar^{1+} ion bombardment has therefore been investigated. By using the well proven and highly sensitive TU Wien quartz crystal microbalance technique (QCM), the sputtering yields of the W samples was measured in-situ under ultra-high vacuum (UHV) conditions. For the investigation of the W fuzz sample, the QCM was installed as a catcher opposite the targetholder and calibration measurements were performed to reconstruct the sputtering yield. Surprisingly, a significantly lower sputtering yield was observed for W fuzz than for smooth W samples. However, this can be well explained by redeposition of the sputtered tungsten in the fibrous structures of the W fuzz.

List of Publications

Parts of this thesis have already been published.

Publications in Scientific Journals:

- R. Stadlmayr, P.S. Szabo, **D. Mayer**, C. Cupak, T. Dittmar, L. Bischoff, S. Möller, M. Rasinski, R.A. Wilhelm, W. Möller and F. Aumayr
  "Sputtering of Nanostructured Tungsten and Comparison to Modelling with TRI3DYN", *Journal of Nuclear Materials*, 532(2020)

- R. Stadlmayr, P.S. Szabo, **D. Mayer**, C. Cupak, W. Möller and F. Aumayr
  "Erosion of iron-tungsten model films by deuterium ion irradiation: a benchmark for TRI3DYN", *Physica Scripta*, T171(2020)

- R. Stadlmayr, P.S. Szabo, B.M. Berger, C. Cupak, R. Chiba, D. Blöch, **D. Mayer**, B. Stechauner, M. Sauer, A. Foelske-Schmitz, M. Oberkofler, T. Schwarz-Selinger, A. Mutzke and F. Aumayr
  "Fluence dependent changes of surface morphology and sputtering yield of iron: comparison of experiments with SDTrimSP-2D", *Nuclear Instruments & Methods in Physics Research Section B*, 430(2018)

- P.S. Szabo, R. Chiba, H. Biber, R. Stadlmayr, B.M. Berger, **D. Mayer**, A. Mutzke, J. Doppler, M. Sauer, J. Appenroth, J. Fleig, A. Foelske-Schmitz, H. Hutter, K. Mezger, H. Lemmer, A. Galli, P. Wurz and F. Aumayr
  "Solar wind sputtering of wollastonite as a lunar analogue material - Comparison between experiments and simulations", *Icarus*, 314(2018)

Conference Contributions:

- R. Stadlmayr, B.M. Berger, D. Blöch, **D. Mayer**, B. Stechauner and F. Aumayr "Erosion of fusion relevant surfaces by using a quartz crystal microbalance", *Proc. of the XXIII International Conference on Ion-Surface Interactions (ISI-2017), editors: E. Yu. Zykova, P.A. Karaseov, A.I. Titov and V.E. Yurasovam, 21.-25.08.2015, Moscow, Russia*, Vol.1, National Research University Higher School of Economics, 2017, S.46-49

Contents

3 Introduction

Technical progress and the associated worldwide increase in energy demand are moving inexorably hand in hand into the future. The majority of the world's energy supplies are covered by fossil fuels such as coal, oil and gas [6, 7], and are thus a crucial driving force behind global warming. The expansion of renewable energies, with hydropower, wind power and solar power as the main representatives, has more than doubled worldwide in the last 10 years [8], but their power output is still significantly lower than that of fossil energy production. Another, mainly CO_2-neutral but more powerful alternative is nuclear power. There are two ways to use nuclear power for energy generation based on the mass defect, one is nuclear fission, in which heavy atomic nuclei are split into lighter nuclei, and the other is nuclear fusion, in which light atomic nuclei are fused into a heavy atomic nucleus. Up to now there are only fission reactors, but their public image is extremely negative due to the terrible accidents in Chernobyl in 1986 and Fukushima in 2011 as well as the serious problem of final storage of the accumulated nuclear waste. But despite the inclusion of these tragic disasters, nuclear energy is by far one of the safest sources of energy [9, 10]. In this respect, great hopes are based on the realisation of nuclear fusion power plants, as they neither produce large amounts of nuclear waste nor pose a potential danger to the environment in the case of a worst-case scenario [11]. However, the technical implementation of nuclear fusion on Earth is a very challenging task, since the fundamental subfield of physics - plasma physics - is still quite young and therefore new phenomena occur from time to time which cannot yet be fully explained by existing theories. Also from a practical point of view, there are huge challenges to overcome, especially in the field of plasma-wall interaction, since the materials used have to withstand the enormous fusion conditions.

Fusion research reactors such as JET, ASDEX Upgrade or JT-60 were key to the feasibility of a future fusion power plant and their research data have significantly contributed to a deeper understanding of plasma physics. Based on these research results, a worldwide collaborative research project ITER was initiated in 2007 and the start of construction of the largest fusion research reactor in Cadarache/Southern France was made.

In the following, a brief summary of fusion research is given to introduce the problems and the importance of the subject area dealt with in this thesis.

3.1 Brief Overview of Nuclear Fusion

The sun generates its energy from thermonuclear fusion reactions, which take place in the core of the celestial body and can only proceed to the required extent at prevailing temperatures in the range of 10^7 K. The high gravity of the solar mass causes the cohesion of the plasma and is called gravitational confinement. The most important thermonuclear reaction is the proton-proton chain [12]:

$$\begin{aligned} \mathrm{p} + \mathrm{p} &\longrightarrow {}^{2}_{1}\mathrm{D} + \mathrm{e}^{+} + \nu_{\mathrm{e}}(0.263\ \mathrm{MeV}) + 1.442\ \mathrm{MeV} \\ {}^{2}_{1}\mathrm{D} + \mathrm{p} &\longrightarrow {}^{3}_{2}\mathrm{He} + \gamma + 5.493\ \mathrm{MeV} \\ {}^{3}_{2}\mathrm{He} + {}^{3}_{2}\mathrm{He} &\longrightarrow {}^{4}_{2}\mathrm{He} + 2\,\mathrm{p} + 12.859\ \mathrm{MeV} \end{aligned}$$

Deducting the neutrino energy of 0.526 MeV (due to their low interaction, neutrinos leave the sun and do not contribute to energy generation), a total of 26.2 MeV of thermal energy is released during each of these cycles [13].

However, the process of the starting reaction of two protons into deuterium is initiated by the weak interaction, which is why the cross-section and thus also the reaction rate is very small (the average lifetime of a proton in the nucleus of the sun is about $7.9 \cdot 10^9$ a).

3.1.1 Realisation of Nuclear Fusion on Earth

It is the aim of controlled nuclear fusion to simulate the conditions that prevail inside stars by means of hot plasmas in fusion reactors. The binding energy released in the nuclear reactions will be transformed into electrical energy [14].

Since, on the one hand the fusion process of the sun takes far too long and, on the other hand the gravitational pressure prevailing there, which is necessary for fusion, is unattainably high, an alternative way to fusion on earth is needed. The most promising alternative fusion reaction is the following [15]:

$$ {}^{2}_{1}\mathrm{D} + {}^{3}_{1}\mathrm{T} \longrightarrow {}^{4}_{2}\mathrm{He}(3.5\ \mathrm{MeV}) + \mathrm{n}(14.1\ \mathrm{MeV}) $$

Compared to other possible reactions such as D-D fusion, this reaction has the largest cross section or reaction parameter and it has been shown that a D-T plasma with a density n_{DT} of 10^{20} m^{-3} must have a temperature of 10 - 15 keV [14, 16].

However, it should be mentioned that even this effective cross-section is so small that the mean free path for fusion reactions is of the order of kilometres. To shorten the mean free path, the plasma must be confined. This can be achieved either by MCF (Magnetic Confinement Fusion) or ICF (Inertial Confinement Fusion), whereby the research work towards an MCF type fusion reactor is much more advanced and promising, which is why the ICF type will not be discussed further here.

3.1.2 Magnetic Confinement Fusion

Plasma confinement by magnetic fields is based on the Lorentz force and is realised by sets of coils along a torus-shaped or at least torus-like reaction vessel. The magnetic field is arranged so that electrons and ions of the plasma essentially follow the field lines until they find a reaction partner [17].
However, a strictly toroidal magnetic field is not sufficient to enable confinement. The reason for this is the occurring combined curvature and gradient drift, which forces a charge separation of the particles, whereby an electric field forms and the resulting $\vec{E} \times \vec{B}$ drift transports ions and electrons in the direction of the vacuum vessel.

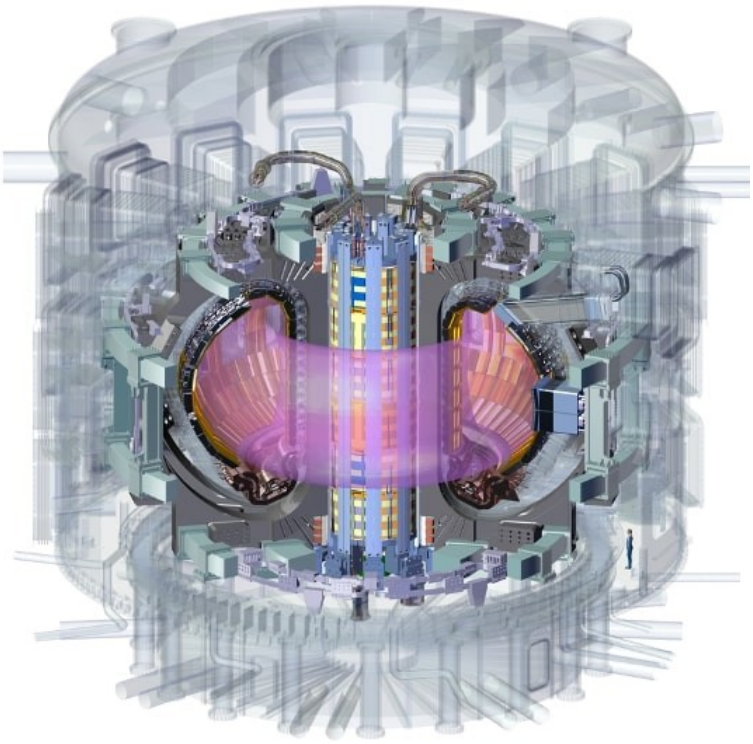

Figure 3.1 – Illustration of the future ITER Tokamak currently being constructed in the south of France. Picture taken from [17].

.

It has been found that this problem can be solved by applying an additional poloidal magnetic field, thus ensuring plasma confinement. This poloidal component can be generated either by a plasma current flowing in the toroidal direction or by an additional special set of coils. In the first case, one speaks of a Tokamak (e.g. JET, ASDEX Upgrade), in the second case of a Stellarator (e.g. Wendelstein 7-X).

Due to the highly complex construction of a stellarator, only a tokamak reactor type can be considered for future reactors such as ITER (see figure 3.1) or, subsequently, DEMO, since these will have to be built considerably larger in order to finally achieve a gain factor $Q > 1$. The amplification factor Q is the ratio between the fusion power and the heating power to be applied and scales with the volume.

3.2 Plasma Facing Materials

The plasma edge region in a fusion reactor faces the biggest material-specific challenges and consists mainly of the first wall and the divertor [18], visualized in figure 3.2. In addition to the enormous thermal loads, which can amount to around $1\,MW/m^2$ at the first wall and even up to $20\,MW/m^2$ at the divertor, the plasma wall components are also exposed to massive neutron and ion impacts and must withstand these without fuel retention [17, 19].

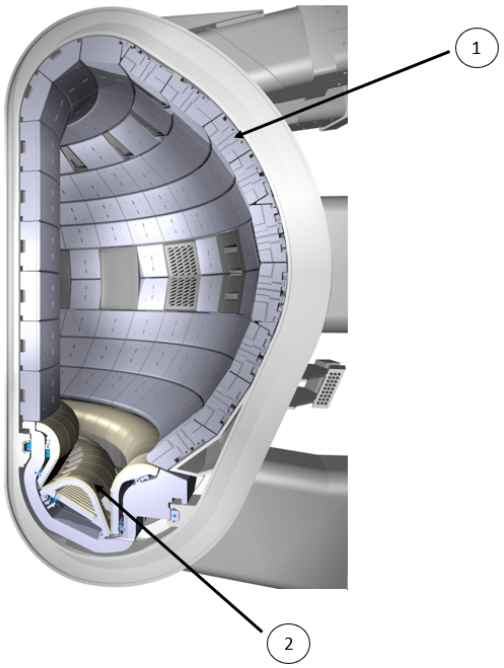

Figure 3.2 – Cross section of the ITER Tokamak Torus provides insight into the plasma-wall interaction zone consisting of the first wall (1) and the divertor region (2). Picture taken from [17].

For the major ITER project, the light metal beryllium will be used for the first wall and tungsten for the divertor. Beryllium is optimally suited as first wall material due to its low atomic number and its resistance to chemical erosion. For the most thermally stressed region in the reactor, the divertor, W is used due to its high melting point, low sputtering yield and low fuel retention. Since W is a high-Z element, even the smallest amounts of it as impurity in the plasma core are critical for the maintenance of the plasma (cooling due to electromagnetic radiation). For this reason, severe erosion of the tungsten components must be prevented under all circumstances. A gas inlet system (Disruption Mitigation System) can be used to admit defined quantities of externally introduced gases, so-called seeding gases (N, Ne, Ar), which sufficiently relieve the tungsten components in the divertor through radiation cooling, so that the sputtering of tungsten can be kept low [17, 20, 21].

3.2.1 W Fuzz

Besides the key positive properties of tungsten, the high melting point, the low sputtering yield and the low tritium retention, there is unfortunately also an undesirable aspect. It has been experimentally found that the surface of a W target exposed to a high He flux ($10^{23} m^{-2} s^{-1}$) at a temperature of 1000 - 2000 K deforms into a fibrous nanostructure which is called tungsten fuzz [2, 3] and can be seen in figure 3.3. The energy of the incident He ions is in the range of 20 - 60 eV, and thus typical for the conditions in the divertor region [19]. This transformation of the surface causes on the one hand a strong reduction of the thermal conductivity and on the other hand the optical reflectivity becomes almost black-body-like [4, 5]. In addition, due to the highly porous and therefore weak structure, one could assume that the sputtering yield of W fuzz is also increased accordingly and thus can cause the release of critical W impurities to plasma.

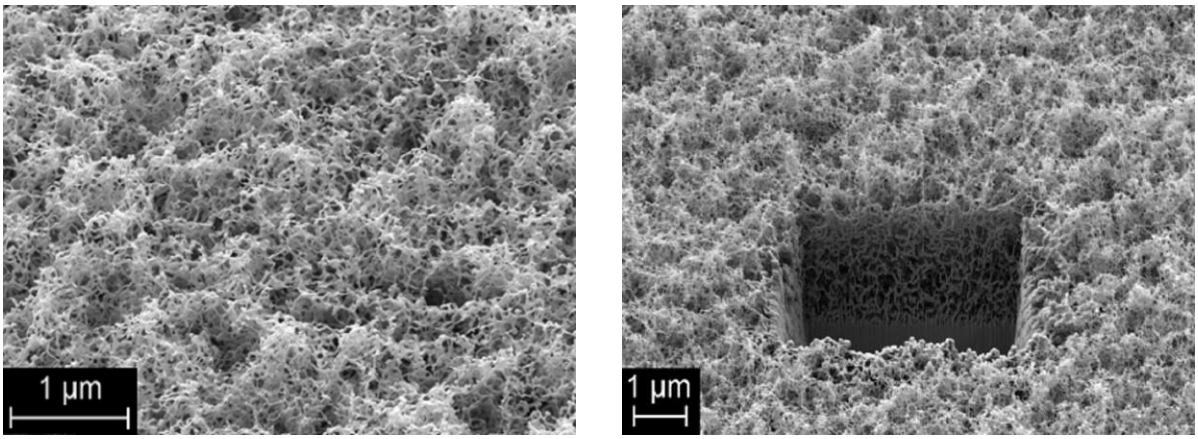

Figure 3.3 – Surface morphology of nanostructered W Fuzz (left) and with focused ion beam (FIB) cut (right) showing the thickness of the Fuzz layer. SEM images performed by Forschungszentrum Jülich (Germany). Picture to the right hand side taken from [22].

.

3.3 Physics of Sputtering

Sputtering is the ejection of target atoms due to energetic particle bombardment and represents the erosion of the target material. When the projectile particles hit the target surface, collision cascades occur, resulting in kinetic momentum transport with the atoms of the layers near the surface. In order to eject a target atom from the surface, the direction of the incoming ion impulse must reverse at least once with respect to the surface normal and a certain energy threshold, which corresponds to the binding energy, must be overcome at the target atom. The number of ejected target atoms $N_{sputtered}$ in relation to the incoming projectiles N_{ions} is defined as sputtering yield Y and is thus the most important parameter for the physical erosion of materials [23, 24].

$$Y = \frac{N_{sputtered}}{N_{ions}}$$

The sputtering yield is mainly dependent on the kinetic energy of the projectiles, the mass ratio between target and projectile atom and the angle of the incident particles. With increasing projectile energy, the sputtering yield increases until it reaches a maximum value. Projectiles with an energy higher than this saturation energy penetrate into deeper layers of the target and therefore contribute less to sputtering of surface atoms.

So far, it was assumed that the ejected target atoms can all leave the target undisturbed and this theoretical consideration is acceptable for sufficiently smooth, flat target surfaces. The situation is much more complicated for rough surfaces, since on the one hand it can occur that individual regions are shadowed and thus no projectiles can hit them (shadowing), or on the other hand that atoms that have already been ejected can reattach to the target surface (redeposition) [22, 25–27].

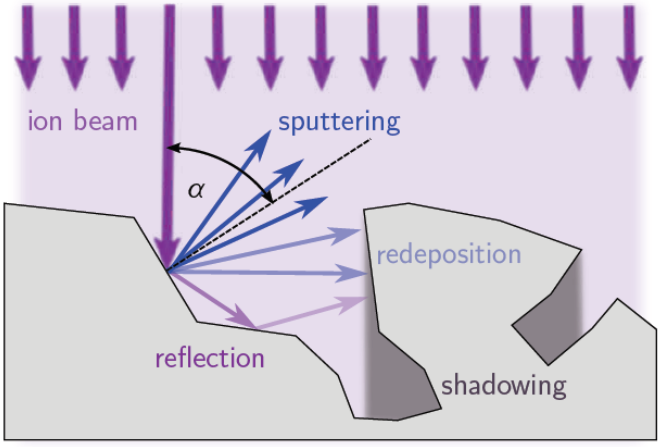

Figure 3.4 – Sputtering process of a rough surface, picture taken from [28].

3.4 Quartz Crystal Microbalance (QCM) Technique

The quartz crystal microbalance represents a well-proven and highly precise in-situ measurement technique for determining the erosion rates of metallic samples to be investigated. This technique is based on Sauerbrey's principle that the resonance frequency f of a quartz crystal operated in shear mode depends on the thickness d_Q of the quartz crystal [29–31].

A change in the layer thickness Δd and thus the mass Δm of the quartz, for example through ion bombardment, therefore results in a change in the resonant frequency Δf, which can be measured very precisely. With this relationship, known as the Sauerbrey equation [29], it is possible to determine the mass change rate of a target material, which is deposited as a thin layer (a few 100 nm) on top of the quartz, in real time:

$$\frac{\Delta f}{f} = -\frac{\Delta d}{d_Q} = -\frac{\Delta m}{m_Q} \tag{3.4.1}$$

The sputtering yield of a target under ion bombardment is determined by measuring the incoming ion current density j_{FC} as well as the time-related frequency change $\Delta f/\Delta t$ [32]:

$$y[amu/ion] = \frac{q \cdot e_0}{j_{FC}} \cdot \frac{\rho_Q \cdot d_Q}{f_Q \cdot m_U} \cdot \frac{\Delta f}{\Delta t} = \frac{1}{j_{FC}} \cdot \frac{\Delta f}{\Delta t} \cdot Const. \tag{3.4.2}$$

Here q is the incident ion electric charge, e_0 the electron charge, ρ_Q the density of the quartz and m_U the atomic mass unit ($1\,m_u = 1.66 \cdot 10^{-27} kg$).

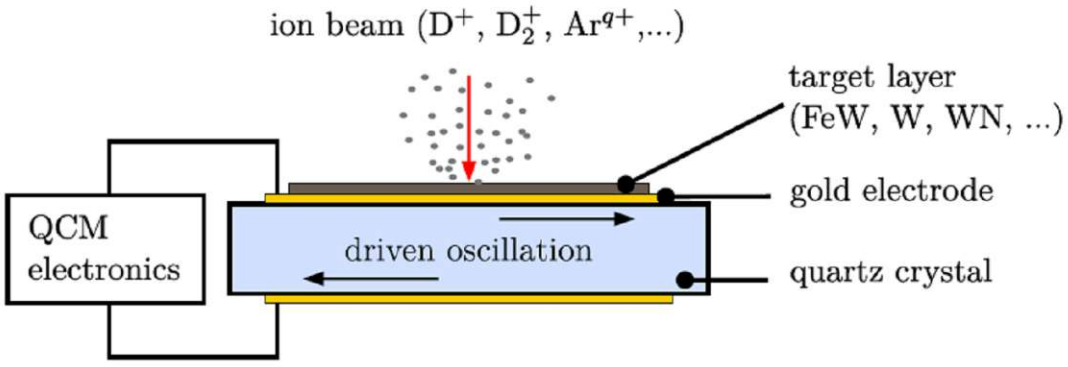

Figure 3.5 – Functional schematic of the QCM technique. Figure taken from [33].

3.5 Motivation

In this chapter, the fundamentals of nuclear fusion research were presented in a short, clear way and the important plasma wall issues were pointed out. The lifetime of plasma wall materials is related to the erosion behaviour of the components. Of special importance is the erosion resistance in the W coated divertor region, as even only small high Z impurities could cause the plasma to extinguish. As already mentioned in chapter 3.2, so-called seeding gases (N, Ne, Ar) are deliberately injected into the reactor vessel by the disruption mitigation system in order to suppress transient events (disruption, Edge Localised Modes) on the one hand and to cool the W divertor region on the other. However, it is also important to investigate what erosion is caused by these seeding gases, such as Ar, at the divertor itself. Since the formation of W fuzz during the burning process cannot be completely avoided, the erosion behaviour of W fuzz in particular is of high interest. For this reason, W and W fuzz samples were investigated under Ar^{1+} ion bombardment in the course of this thesis in order to determine the sputteryield as well as the sputter distribution.

4 Experimental Setup

The fundamental requirements for accurate performance of experiments using any kind of ions as projectiles and material surfaces as targets are ultra-high vacuum condtions. These prevent the neutralization of ions on their way to the target and keep the prepared surface sufficiently clean. For UHV a pressure better than $10^{-8}\,\mathrm{mbar}$ inside the sample chamber is necessary. A rotary-vane pre-vacuum pump and two turbomolecular pumps form the vacuum pump system enable these pressure conditions and thus ensure accurate measurements.

As mentioned in chapter 3.5 singly charged Argon Ar^{1+} ions have been chosen as projectile. High ion fluences of typically $10^{22}\,\mathrm{Ar}^{1+}/\mathrm{m}^2$ are required to provide a comparison with plasma-like conditions. To achieve this, the ion source can generate a temporally stable and continuous ion beam with a pre-defined energy of up to $5\,\mathrm{keV}$. An electric double lens system followed by two pairs of deflection plates allows a focused beam path onto the target and a specific beam profile.

By analyzing the residual gas with a quadrupole mass analyzer, the quality of the measurement environment can be derived from the spectrum of the detected elements. Impurities such as, for example, water and nitrogen molecules, which adhere to the chamber walls as adsorbates, must be reduced to a minimum by baking (heating) the chamber to over 100 degrees centigrade for several hours.

For the experimental investigations a well-proven and already installed laboratory system was used, which perfectly fulfils the mentioned requirements. However, some changes were made to further optimize the quality of the measurements and to enable the experimental approach to solve the defined tasks of this diploma thesis. The modifications that have been made to the existing chamber system, which include the installation of a Wien velocity filter and the integration of the TU Wien QCM Catcher system are described in detail in chapter 4.1.

Now that the technical requirements for the experimental realisation of the task have been summarised above, the measurement challenges still need to be overcome. An experiment can only provide a reliable result if the system and the conditions that led to this result are known. Therefore the measurement setup concerning the essential aspects of ion beam diagnostics and the sensitive QCM electronics is discussed in detail in chapter 4.2.

4.1 Sample Chamber Modifications

4.1.1 Wien Velocity Filter

An open problem in the otherwise very solid setup is the straight geometric arrangement of the ion source to the target, so that unwanted particle bombardment by neutralized projectiles is also possible. The simplest approach would be to shift the target position by an offset from the center in X and Y direction, so that there is no in-line alignment between source and target anymore. This would, however, have the disadvantage that the ion beam would basically have to be deflected by the electronic optics in order to hit the target, resulting in a slight decrease in the ion current density. And since the electric lens system is only energy selective, it would still be possible for other projectiles like Ar^{2+} to hit the target.

A good remedy is the use of a Wien velocity filter, which eliminates multiple charged ions like Ar^{2+} or Ar^{3+} and ions of impurities. The Wien Filter, which is mounted between the ion source and the electric lens system, also has an inclination of the optical axis of 1.2 degrees, which leads to a suppression of the neutral particles. The only disadvantage is the extension of the ion path, resulting in a slightly smaller ion current.

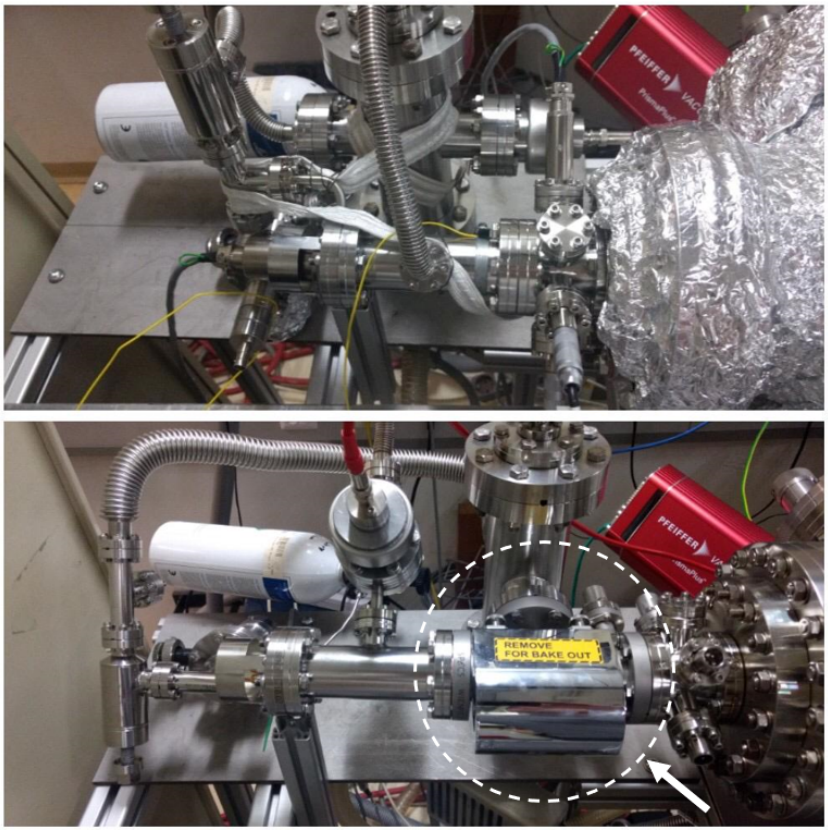

Figure 4.1 – Chamber setup without (top) and with Wien Filter (bottom, encircled).

4.1.1.1 Basic Principle

A charged particle moving with the velocity $\vec{v}$ through an electrical field $\vec{E}$ and a magnetical field $\vec{B}$ experiences the Lorentz force $\vec{F_L}$. This leads to a deflection of the particle path, unless the contributions of the Lorentz force cancel each other out and the acting force vanishes. And exactly this approach describes the basic principle of a Wien filter and the criterion which a charged particle has to fulfil in order to pass is given as follows:

$$\vec{F_L} = q(\vec{E} + \vec{v} \times \vec{B}) \stackrel{!}{=} \vec{0} \tag{4.1.1}$$

From a technical point of view, the electric field $\vec{E}$ is generated by a plate capacitor and the magnetic field $\vec{B}$ by a permanent magnet, so that $\vec{E} \perp \vec{B} \perp \vec{v}$ with $|\vec{E}| = E, |\vec{B}| = B$ and $|\vec{v}| = v$. The kinetic energy E_{kin} of an incoming particle with charge state q, which was driven by the beam acceleration voltage U_{Beam} and the electrical field E of a plate capacitor with d being the distance between the deflection plates and U_D being the deflection voltage, are given by:

$$E_{kin} = \frac{1}{2}mv^2 = qU_{Beam} \qquad \text{and} \qquad E = \frac{U_D}{d} \tag{4.1.2}$$

With 4.1.1 and 4.1.2 the mass m of the particle is determined by:

$$qE = qvB \qquad \Rightarrow \qquad \frac{m}{q} = 2U_{Beam}e_0B^2d^2\frac{1}{U_D^2} \propto \frac{1}{U_D^2} \tag{4.1.3}$$

and since B is a constant due to the permanent magnet ($B = 460mT$), the mass over charge state relation of the particle remains only as a function of the deflection voltage U_D. Thus the particle selection can be set by controlling the deflection voltage.

4.1.2 Catcher Setup

Due to their complex microscopic structure, materials such as tungsten fuzz cannot be applied as a thin layer on a target quartz crystal. All of their characteristic properties such as porosity and surface roughness would be lost, making it impossible to determine their erosion rates directly with the well-proven QCM technique. Therefore the so-called catcher system was developed at TU Wien in 2018 [33]. In this setup the QCM acts as a catcher for sputtered target particles. Captured target particles lead to an increase in mass of the catcher crystal, which can be calculated by measuring the reduction of the resonant frequency.

The basic principle of the catcher setup is shown in figure 4.2. An incident ion beam with well-defined energy hits the target sample at an angle of incidence α with respect to the surface normal and causes sputtering of target material. For accurate positioning of the sample, the target holder is attached to a xyzα - manipulator. The Catcher QCM is mounted opposite the target holder, adjustable in x - direction and is distanced at a spacing d from the target. The sputtered target particles can stick to its surface and lead to a mass increase of the quartz-crystal. Thereby the sticking coefficient, which is the ratio of the number of particles adhering to the surface of the catcher to the total number of particles hitting it, can be assumed to be 1 for same material elements. For this reason, the same element as the target material is chosen for the catcher material.

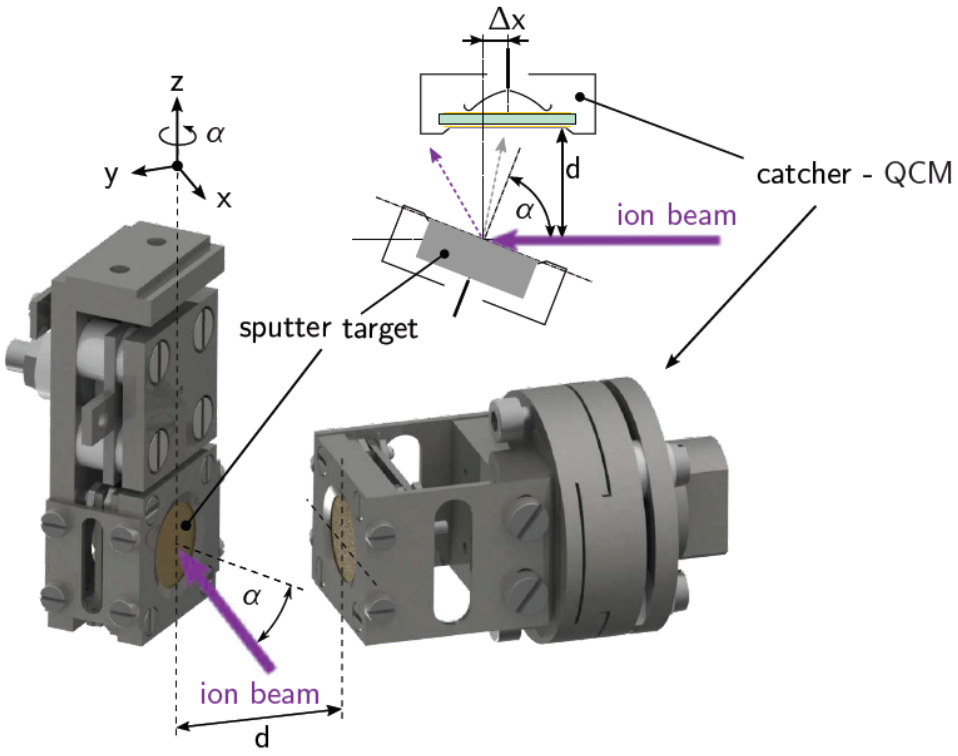

Figure 4.2 – Catcher setup illustrated as a 3D drawing created by R. Stadlmayr et.al. [28]. An ion beam impacts the target sample at an angle α. The target holder is attached to an xyzα-manipulator to optimally position the target for the corresponding measurement. Opposite the target holder, at a distance d, the catcher QCM is located, whose surface normal is perpendicular to the ion beam direction. The shift Δx can be adjusted via the manipulator of the target holder. In the course of required calibration measurements, a second QCM operates on the target side. Figure taken from [28].

However, it must also be taken into account that a small part of the ion beam is reflected at the target surface and may cause sputtering at the catcher surface, which in turn is associated with a mass decrease of the catcher QCM. The theoretical evaluation of the catcher's mass change rate y_C has been derived in reference [33, 34] and results as follows:

$$y_C[amu/ion] = q \cdot \frac{C}{\overline{I_{FC}}} \cdot \frac{A_{FC}}{A_{Beam}} \cdot \left(\frac{\Delta f}{\Delta t}\right)_{Catcher} \tag{4.1.4}$$

In this formular q is the charge state of the ion projectiles, $\overline{I_{FC}}$ is the mean ion current measured at the FC, A_{FC} denotes the FC's area and A_{Beam} is the area of the beam profile. The constant C includes material properties of the quartz crystal and $\Delta f\ /\Delta t$ is the measured signal change of the catcher QCM.

To reconstruct the erosion rate of the target material from the measured catcher data in an experimental approach, specific calibration measurements are necessary. Therefore a second QCM is used, but on the target side, so that now two QCMs are working simultaneously. Since the target QCM is irradiated directly by the ion beam, absolute sputteryield measurements are possible and thus allow a calibration of the catcher signal by determining the ratio between the mass changes of the catcher QCM and the target QCM. This calibration factor is called the g parameter:

$$g(\Delta x, \alpha, d) = \frac{y_C(\Delta x, \alpha, d)}{y_T(\alpha)} \tag{4.1.5}$$

If the profile of g is determined experimentally by varying one of the three dependencies Δx, α or d (for the definition of these parameters see 4.2) and fixing the other two, the catcher measurement even enables the reconstruction of a sputtering distribution of the target material. If, after these calibration measurements, a sample with unknown or complex surface properties but from the same element is used instead of the target quartz crystal, y_C and g can be used to extrapolate the target's sputtering yield y_T [35].

4.2 Measurement Setup

The key to success of physically relevant results from experimental measurements is on the one hand a precise measuring technique and on the other hand an exact measuring procedure. Since the selection of the ion projectiles is already controlled by the Wien Filter, the measurement setup must essentially cover the characterization of the ion current, by measuring both the ion current density and the ion beam profile and the integration of the sensitive QCM technique.

In order to achieve a constant ion current for the entire measurement, it is essential that the ion source is already in thermal equilibrium. For this purpose, the temperature of the ion source is permanently measured via a thermocouple. Only after reaching the operating temperature of about 60-70 $°C$ (depending on the working gas pressure) there are no more temperature fluctuations and the source is ready to generate a constant ion current. The detection of the incident ion beam, by measuring both the ion current and the beam profile, is described in detail in chapter 4.2.1.

Integrating the QCM requires high precision electronics that can measure high frequencies in the MHz range with an accuracy of mHz to resolve the small frequency changes caused by sputtering. Furthermore, the electronics must be capable to operate two QCMs simultaneously in order to perform the required calibration measurements, in which a QCM is used both on the target side and on the catcher side. In 4.2.2 these important issues are discussed and the QCM electronics used for this purpose are described.

The measuring procedure of a new, unirradiated sample starts with cleaning the sample surface by a scanned ion beam, since during the sample preparation in air, impurities may have adhered to the surface or oxides may have been formed. Due to the sputtered adsorbates, the detected QCM signal is significantly increased and would therefore falsify the measurement results. The purpose of the QCM measurements is to investigate the erosion behaviour of the target material by ion bombardment. Therefore the required measurement series can now be divided into 3 main parts:

- Specific measurements before irradiation $\rightarrow y_{C,before}(\Delta x, \alpha, d)$
- Irradiation of the sample ($\Phi \approx 10^{21}...10^{22}\,\mathrm{Ar}^{1+}/\mathrm{m}^2$)
- Specific measurements after irradiation $\rightarrow y_{C,after}(\Delta x, \alpha, d)$

According to chapter 4.1.2, the catcher yield y_C depends on the ion angle of incidence α and on the two catcher parameters Δx and d, so the specific measurements examine the dependencies of the y_C by varying one of the parameters and fixing the others, leading to the resulting functions $y_C(\Delta x; \alpha, d)$, $y_C(\alpha; \Delta x, d)$ and $y_C(d; \alpha, \Delta x)$.

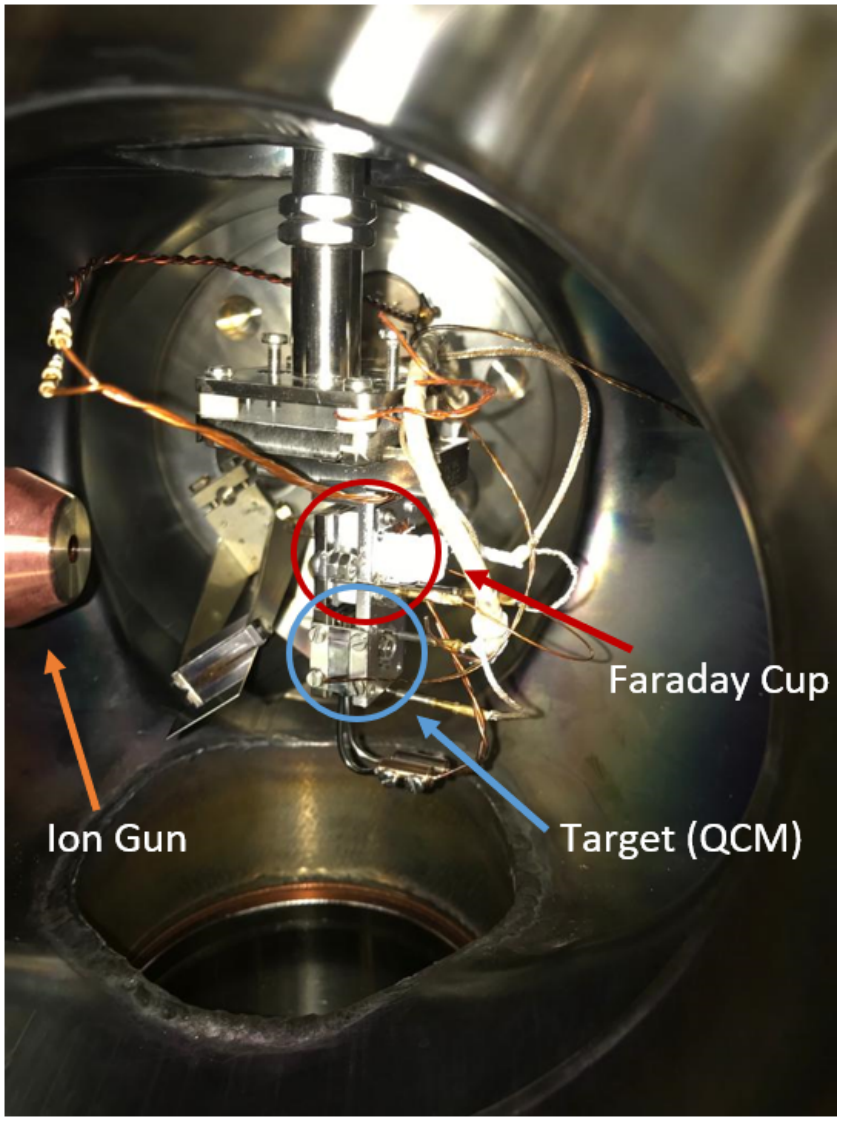

Figure 4.3 – Inside view of the chamber showing the target holder attached to a xyzα-manipulator. The target QCM (blue) is located at the bottom, the Faraday Cup (red) for measuring the ion current is located directly above. Note that the perspective is from the catcher's point of view and during measurement, the target surface would face the catcher, of course (other than in this position).

4.2.1 Ion Beam Profile Detection

To obtain accurate measurements, it is essential to determine and adjust the ion beam profile as accurately as possible. The ion current is detected by a Faraday Cup, which is mounted right above the target holder, and read out by a picoamperemeter. To prevent secondary electrons from escaping from the Faraday Cup, which would lead to measurement inaccuracies, an attractive potential of +50V was applied between FC and picoamperemeter by using a suppressor. Since the FC is not mounted at the same height (z-axis) as the target, the sample holder has to be moved for each current measurement. In addition, the current measurement at the FC can only be performed under normal incidence of the ion beam, meaning $\alpha = 0$. In order to determine the shape of the ion beam profile, the current at the FC is measured at mm intervals in $\pm y$ and $\pm z$ direction starting from the center point, so that a cross-shaped measuring grid is scanned. At the beginning of each measurement, the ion source parameters are adjusted and optimized in this way until the positioning and the profile of the ion beam are achieved at the maximum possible current intensity.

A current measurement is always performed both before and after sample irradiation in order to take any current drift into account in the calculation of the erosion rate. It has been proven that the source used delivers a very constant ion current and has also remained stable over days during measurements. Furthermore, the ion source is capable of generating very sharp ion beam profiles, which means that the current drops very steeply at the edge and thus resulting in well-defined beam profiles.

Basically two types of different current profiles were used in the course of the measurements that were performed:

4.2.1.1 Scanned Ion Beam Mode

Especially for calibration measurements, where a second QCM is used on the target side as mentioned in chapter 4.1.2, the ion beam must be scanned uniformly over a critical area (active area) so that the sensitivity of the QCM becomes independet of the quartz area that is hit by the ion beam [30]. The ion source allows to scan the ion beam over an area of up to $10 \times 10\, mm^2$ with a step size of 0.1 mm and a typical time per dot of 50 μs. A scanning area of $5 \times 5\, mm^2$ was typically used for the experiments and the variation of the current intensity along the applied surface could always be kept below 10 %. At the boundary, the FC current drops steeply by an order of magnitude and finally approaches zero within the next tenth of a millimeter, thus providing accurate measurements.

4.2.1.2 Intense Ion Beam Mode

Besides the main advantage of the catcher setup to be able to investigate arbitrarily shaped samples with unknown surface properties, it is also no longer necessary to scan the ion beam with this measuring method. Therefore, intensive, focused ion beams are now also possible, thus reducing the beam time to apply a certain fluence. However, the evaluation of the current profile using the FC measuring method becomes more difficult, since the beam diameter of the focused ion beam is smaller than the FC diameter, resulting in a convoluted current profile.

For this purpose, a MATLAB® routine was written to reconstruct the deconvoluted, real current density profile. As mentioned in 4.2.1, current measurements in $\pm y$ and $\pm z$ direction were performed both before and after each irradiation, but with a smaller step size of 0.25 mm. Since the natural beam profile of the ion source is Gaussian, a Gaussian function was fitted to the measured current values in order to create the convoluted profile ψ. In an one-dimensional approach the FC is modeled as a simple stepfunction $A(r)$, which has the value 1 in the range -0.5 $\leq r \leq$ 0.5 and 0 everywhere else along the radial direction. A Gaussian, normalized initial test function $\varphi(r)$ has now been optimized until the convolution with $A(r)$ yields the final measurement function $\psi(r)$. Therefore equation 4.2.1 has to be satisfied [36].

$$(\varphi * A)(r) = \int \varphi(\tau) A(r-\tau) d\tau \stackrel{!}{=} \psi(r) \tag{4.2.1}$$

This equation can now first be rewritten by using the commutativity of the convolution with $(\varphi * A)(r) = (A * \varphi)(r)$ and in a second step simplified by exploiting the property of the step function [36].

$$\int \varphi(\tau) A(r-\tau) d\tau \stackrel{1.}{=} \int \varphi(r-\tau) A(\tau) d\tau \stackrel{2.}{=} \int_{-0.5}^{0.5} \varphi(r-\tau) d\tau = \int_{r-0.5}^{r+0.5} \varphi(\tau) d\tau \tag{4.2.2}$$

Since $\psi(r)$ represents the measured FC current at the FC position r, the deconvoluted function $\varphi(r)$ must therefore be the current density profile of the incident ion beam.

$$\Rightarrow \psi(r) = \int_{r-0.5}^{r+0.5} \varphi(\tau) d\tau \tag{4.2.3}$$

The numerical calculation of a convolution corresponds algebraically to a polynomial multiplication and formula 4.2.1 in discrete consideration thus becomes [37]:

$$(\varphi * A)(k) = \sum_j \varphi(j)A(k-j) \stackrel{!}{=} \psi(k) \tag{4.2.4}$$

In figure 4.4 a reconstructed current density profile of the incident ion beam is shown, based on the measured FC current values. With the extracted $\varphi(r)$ it is now easily possible to determine the total current of the ion beam by integrating $\varphi(r)$ over the entire radial range.

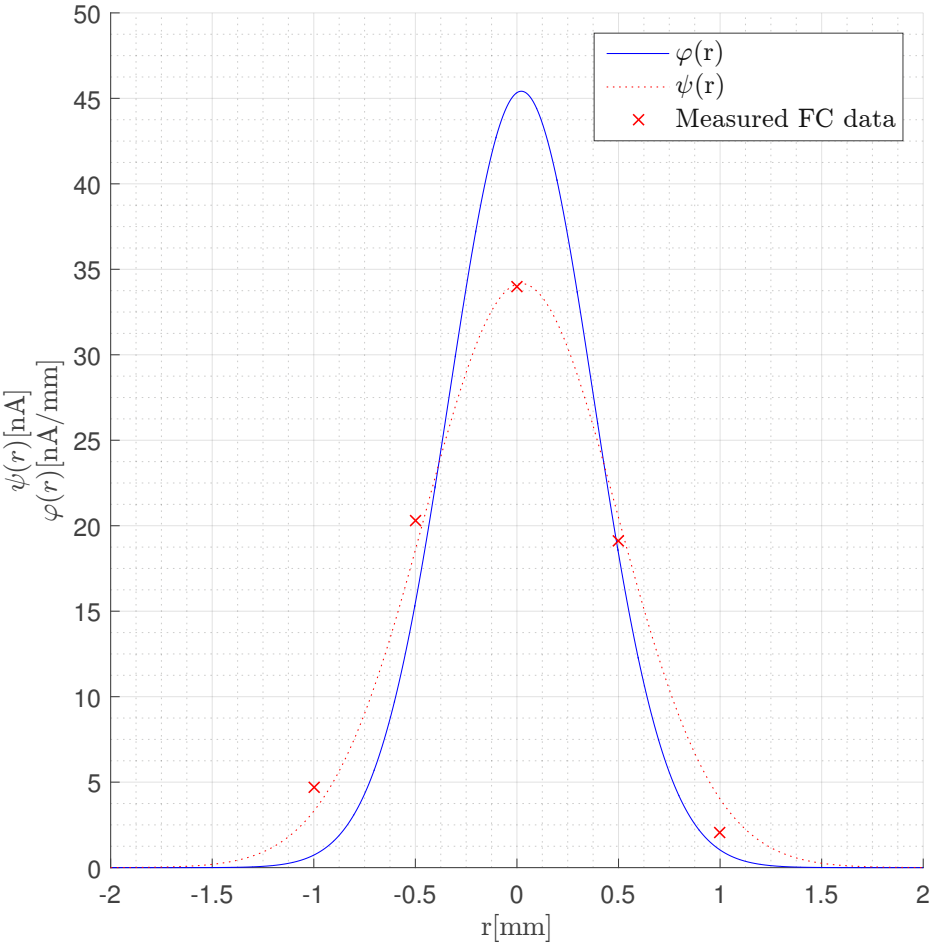

Figure 4.4 – Reconstructed 1D ion beam profile: Based on the FC current measurement points, a Gaussian fit $\psi(r)$ was created, which is the convoluted current profile along the r axis. Using MATLAB®, the fundamental current density profile $\varphi(r)$ of the ion beam could be extracted.

4.2.2 Integrating the QCM

Since the change in mass of the quartz crystal can be determined by its change in frequency, the measuring accuracy is primarily determined by the exact frequency determination [30]. For this purpose M. Schmid [38] has developed the high-precision QCM electronics, which enables frequency measurements of high-frequency input signals in the mHz range.

Via a function generator a sine wave with the initial frequency in the range of the resonance frequency of the quartz is fed into the phase box, as can be seen in figure 4.5. The phasebox now compares the phase difference between drive-voltage of the quartz crystal and the current flowing through it. In series resonance, current and voltage are in phase and the output voltage of the phase box is zero. Thus any deviation from resonance leads to a phase difference and the output signal deviates from zero. The output signal is transmitted via a fast ADC to the PC, where a Python script, written by Stadlmayr R. [39] determines the new input signal for the function generator, so that the crystal is constantly in resonance. The quartz drift and the electronic noise limit the measurement sensitivity of the frequency change to about 10mHz.

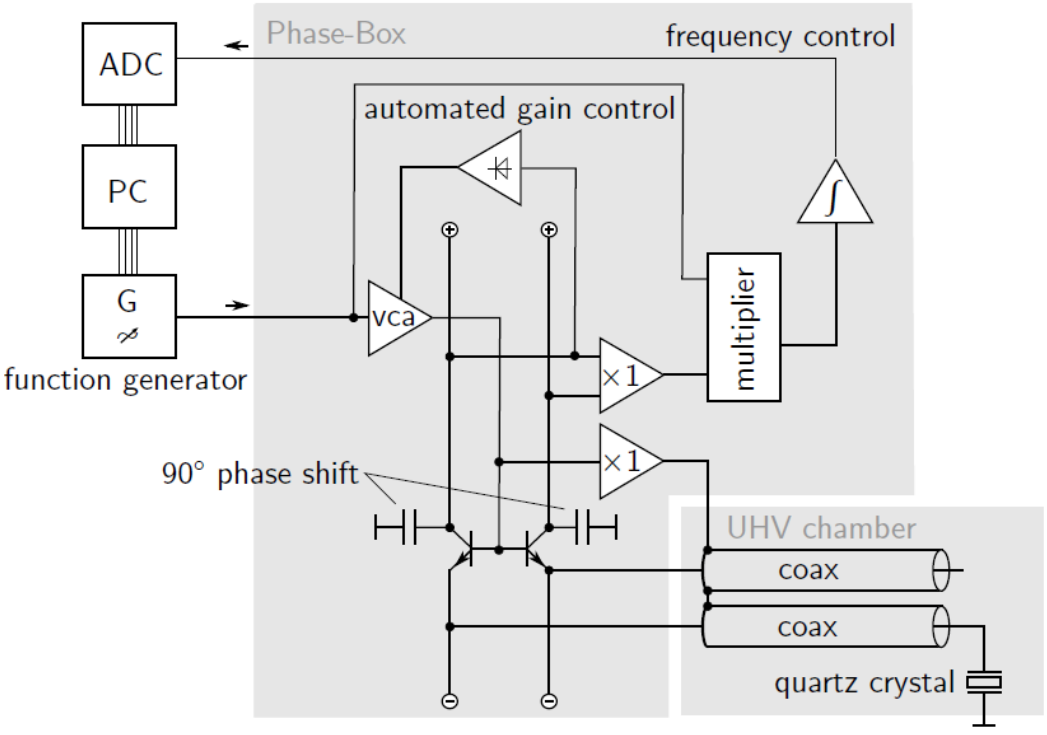

Figure 4.5 – Schematics of the electronic setup for driving the QCM. The phase box, which contains the QCM electronics, is the heart of the QCM setup and ensures that the quartz crystal is kept at its resonance frequency. Figure taken from [28].

5 Results

In this chapter, the experimental results for the investigation of the sputtering behavior of thin, smooth W layers, as well as of W fuzz, are presented and discussed. As already mentioned in chapter 3.2, W is the top material of choice for the usage as a plasma-facing component due to its element-specific properties [1, 18, 40]. In order to handle the enormous local heat loads, especially in the divertor region, so-called seeding gases such as N, Ne or Ar are injected, which relieve the PFCs thermally via radiation cooling [41]. For this reason, Ar^{1+} projectiles were chosen for the following experiments, which hit the W targets with a kinetic energy of 500eV and 2keV, respectively, to better determine and estimate their erosion behavior by the seeding gas itself.

Sample preparation of the smooth W samples was performed by IPP Garching (Germany), where W film thicknesses of about 400 - 500 nm were deposited on polished quartz crystals via a magnetron sputter deposition device. The W fuzz samples were prepared at the PSI - 2 linear plasma device at the Forschungszentrum Jülich (Germany). For this purpose, original W plasma facing component tiles, with a surface area of $10 \times 10\,mm^2$ were exposed to a He plasma with a He flux of $10^{21}\,m^{-2}\,s^{-1}$ and a temperature of 1000 K satisfying the conditions for the fuzz forming regime, already discussed in chapter 3.2.1.

For the measurement of the W Fuzz samples, the new QCM Catcher setup was used [35], in which the determination of the sputtering yield of a bulk material, such as W Fuzz, can be evaluated indirectly by collecting the sputtered particles with an opposing catcher quartz. In order to get sticking coefficient close to 1 [34, 42], a smooth W coated quartz crystal was used as catcher. First, a proof-of-principle measurement was initialized with another W coated quartz crystal instead of the W fuzz sample to determine the g parameter, which represents the ratio between catcher yield and target yield mentioned in 4.1.2. Thus, in this measurement, two QCMs were operated simultaneously, allowing evaluation of both the sputtering yield of the target and that of the catcher.

5.1 Ar^{1+} on W at 500 eV

5.1.1 Classical QCM setup

Using the classical QCM setup, the sputtering yield of a smooth W sample exposed to 500 eV Ar^{1+} ion bombardment at an ion impact angle of 60°(with respect to the surface normal) was investigated. The root mean square roughness of the unirradiated (virgin) sample was previously quantified by atomic force microscopy (AFM) measurements to 7 nm and indicates the smoothness of the W sample surface.

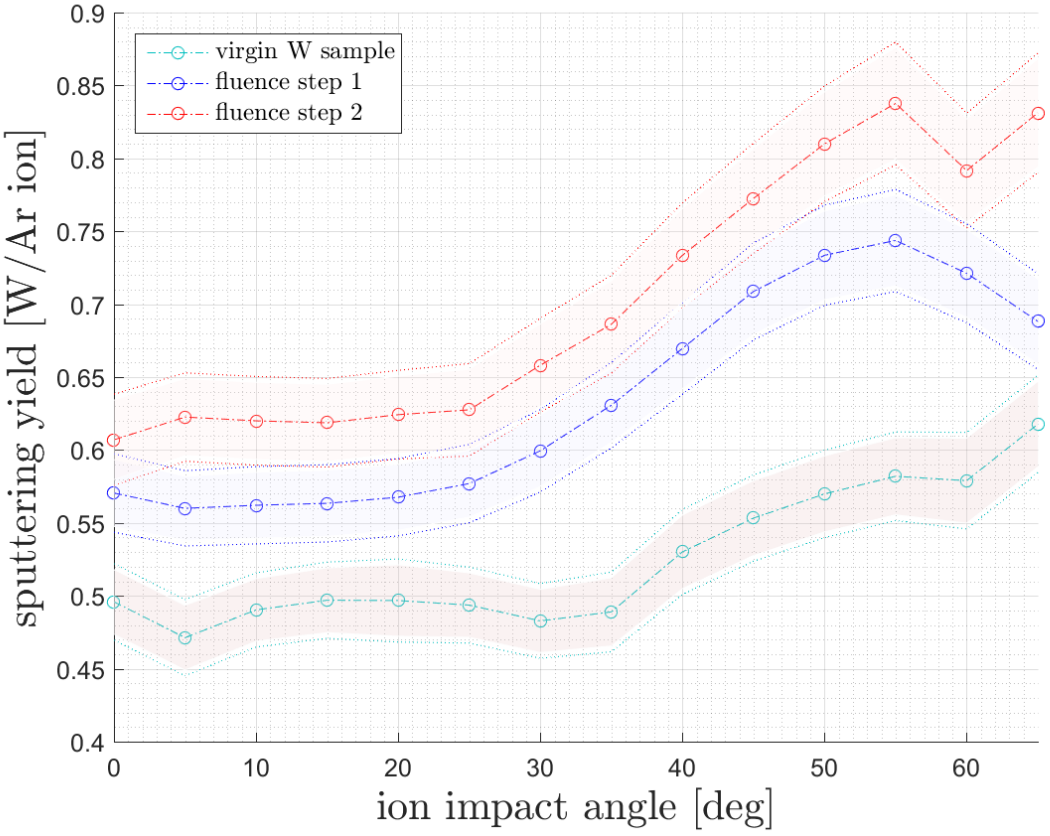

Figure 5.1 – Sputtering yield of a flat W surface as a function of the ion impact angle with respect to the surface normal under 500 eV Ar^{1+} ion bombardment. Ar^{1+} fluences of about $2{,}98 \cdot 10^{21}$ Ar/m² (step 1) and $0{,}99 \cdot 10^{22}$ Ar/m² (step 2) were applied. The colored areas represent the sputter yield relative error.

To achieve precise measurement results, one angular measurement (by rotating the target holder via the manipulator by α) from $\alpha = 0° - 65°$ and one from $\alpha = 65° - 0°$ were performed after each applied fluence step, with α being the angle of ion impact on the target with respect to the surface normal. These were accompanied by measurements of the ion current before and after each individual angular measurement to also consider the stability of the ion beam source. In addition to the variance of the ion beam density, the quartz drift and the Faraday Cup aperture were also included in the measurement results. For more details on error estimation in QCM sputteryield measurements, see [39].

The measured sputtering yield shows a fluence dependence , i.e. the yield slightly increases with increasing fluence as can be seen in figure 5.1. An applied Ar^{1+} fluence of $0{,}99 \cdot 10^{22}\,Ar/m^2$ in total (after fluence step 2) reveals the well known, characteristic sputtering behavior of a smooth W sample [32]. A maximum sputtering yield of $0{,}84 \pm 0{,}05$ W/Ar ion can be observed at an angle of incidence of 55°with respect to the surface normal.

5.1.2 QCM catcher setup

As mentioned in chapter 3.5 the main concern of this research work is the erosion investigation of the W fuzz samples. However, due to the complex and highly porous surface morphology [43, 44], it is not possible to deposit a W fuzz layer as a target substrate on a quartz crystal, as is the case with conventional W samples, and as a result it cannot be investigated using the classical QCM technique. With the QCM catcher setup described in chapter 4.1.2, it is possible to determine erosion rates of bulk materials, such as W Fuzz. In contrast to the classical setup, the sputtered particles of the target are caught by a QCM, which is positioned opposite the target. The manipulator of the target holder allows to observe the catcher behavior in case of a variation in ion beam direction Δx, as well as the behavior in case of change of the incoming ion impact angle α with respect to the target's surface normal. Furthermore, the distance d between target and catcher quartz can also be varied via a set screw on the catcher apparatus. Figure 5.3 illustrates the catcher setup for a visual understanding.

Since the catcher QCM covers only a part of the solid angle, the resulting catcher signal can only be interpreted as a relative sputteryield. On the one hand the signal increases with the numbers of captured target particles but on the other hand decreases due to sputtering caused by reflected ions. The relationship between the detected catcher signal and the actual sputtering yield is determined experimentally by a reference measurement in which a QCM is operated simultaneously on the target side.
Within this reference measurement, the W coated quartz crystal from the previous measurement 5.1.1 is operated again in the target QCM and another, nearly similar W coated quartz crystal is operated in the catcher QCM in order to realize a sticking coefficient of 1 in a good approximation [34, 42].

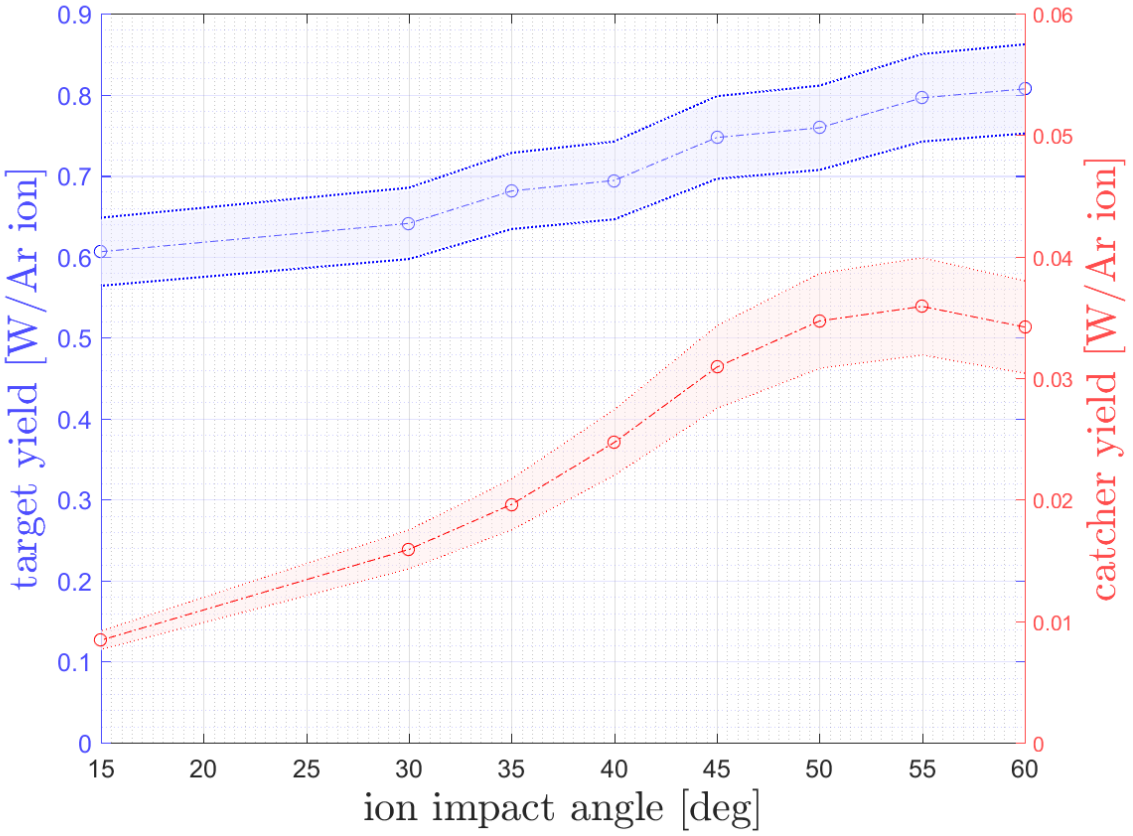

Figure 5.2 – Repeating the same measurement as in 5.1.1 but using the catcher setup, where two QCMs were operated simultaneously allowing evaluation of both the sputtering yield of the target (blue) and of the catcher (red). The catcher parameters were set to: $\Delta x = 1\,\text{mm}$ and $d = 13\,\text{mm}$. The measurement was initiated at an ion impact angle $\alpha = 15°$, since at normal incidence the catcher would be oriented normal to the target. In the angle range 50° - 60°, the pickup rate of the catcher is highest and consequently the signal is strongest. The colored areas indicate the sputtering yield relative errors.

Figure 5.2 shows the comparison of catcher QCM to target QCM of the W coated samples under 500eV Ar^{1+} ion bombardment as a function of the angle of incidence α. At normal ion impact on the target $\alpha = 0°$, it should be noted that the catcher QCM is directed perpendicular to the target QCM, which means that no target particles can be collected and the catcher signal accordingly experiences no changes. Therefore, the angle measurements for the catcher setup were initiated at 15° and regularly performed in 5° steps starting at 30°.

The values for the other two catcher parameters Δx and d were taken from a previous catcher measurement [35]. As can be expected, the catcher signal is significantly lower than the target signal, since only a certain amount of sputtered target particles are caught by the catcher QCM. According to the function profile, the catcher signal is strongest at an ion impact angle between 50° and 60° with respect to the target's surface normal, which means that the pickup rate is highest here. It is important to mention again that only the target holder was rotated by the corresponding angle, the catcher device was fixed in position.

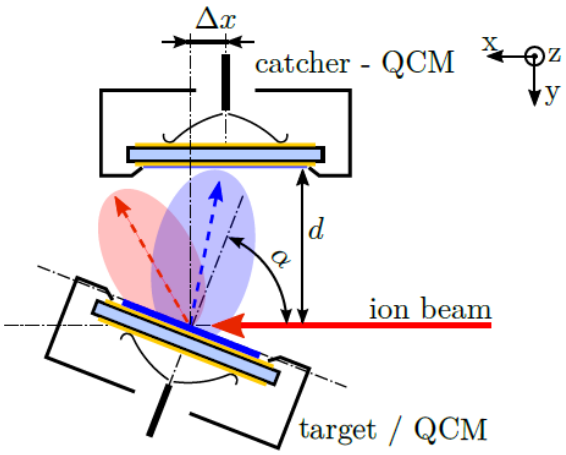

Figure 5.3 – Principle of the catcher setup with two simultaneously operated QCMs. The Ar^{1+} ion beam hits the W coated target quartz crystal at the angle of incidence α and leads to sputtering of W surface particles (blue cone) or the ions are reflected at the target surface (red cone). Opposite the target QCM, the catcher QCM is positioned at a distance d, which collects the sputtered target particles. The target manipulator allows the relative displacement Δx to the catcher to be optimally adjusted so that the catcher signal is strongest, picture taken from [33].

5.2 Ar^{1+} on W at 2 keV

After initial test measurements with the W fuzz target under 500 eV Ar^{1+} ion bombardment, it was observed that the catcher signal remained almost unchanged even under various variations of the parameters Δx, d or α and any potential frequency changes could not be distinguished from the background noise of the quartz oscillation. The possibility of a thin oxide layer formation at the fuzz surface, which could dampen the sputtering yield of the sample at the beginning and thus be responsible for the weak signal, was excluded by an irradiation time of 3200s with an ion flux of $2{,}53 \cdot 10^{15}\,\mathrm{Ar/m^2/s}$. Only by increasing the kinetic energy of the ion beam up to 2 keV a frequency change of the catcher signal could be observed with reasonable certainty. Consequently, despite its porous structure, the W fuzz sample seems to have a lower erosion rate than the smooth W sample before, contrary to expectations.

In order to properly investigate the W Fuzz sample, it was necessary to perform new reference catcher measurements with 2 keV Ar^{1+} ions, which are described in detail in this section. Since the changes in the catcher signal are significantly weaker due to the apparently lower sputtering yield when investigating W Fuzz, it is therefore even more important to evaluate the optimal catcher parameters in order to be able to measure the strongest possible catcher signal. Thus, the fuzz target was replaced again by the W coated quartz crystal and the sample was exposed to a 2 keV Ar^{1+} ion bombardment.

First, an angular measurement was performed again, in which the ion incidence angle on the target was varied in the range 15 to 60 degrees. Figure 5.4 shows a maximum sputtering yield of $1{,}97 \pm 0{,}13\,\mathrm{W/Ar}$ for the smooth W sample at an incidence angle of alpha 60° with respect to the target's surface normal. The slightly higher sputtering yield at 15° compared to the value at 30° is due to a possible impurity layer caused by aeration during sample change, which is sputtered more easily at the beginning of irradiation. As one would expect, the catcher signal shows the same characteristic as in the 500 eV measurement and is most significant for the angular range between 50° and 60°. The other two catcher parameters were again set to $\Delta x = 1\mathrm{mm}$ and $d = 13\mathrm{mm}$.

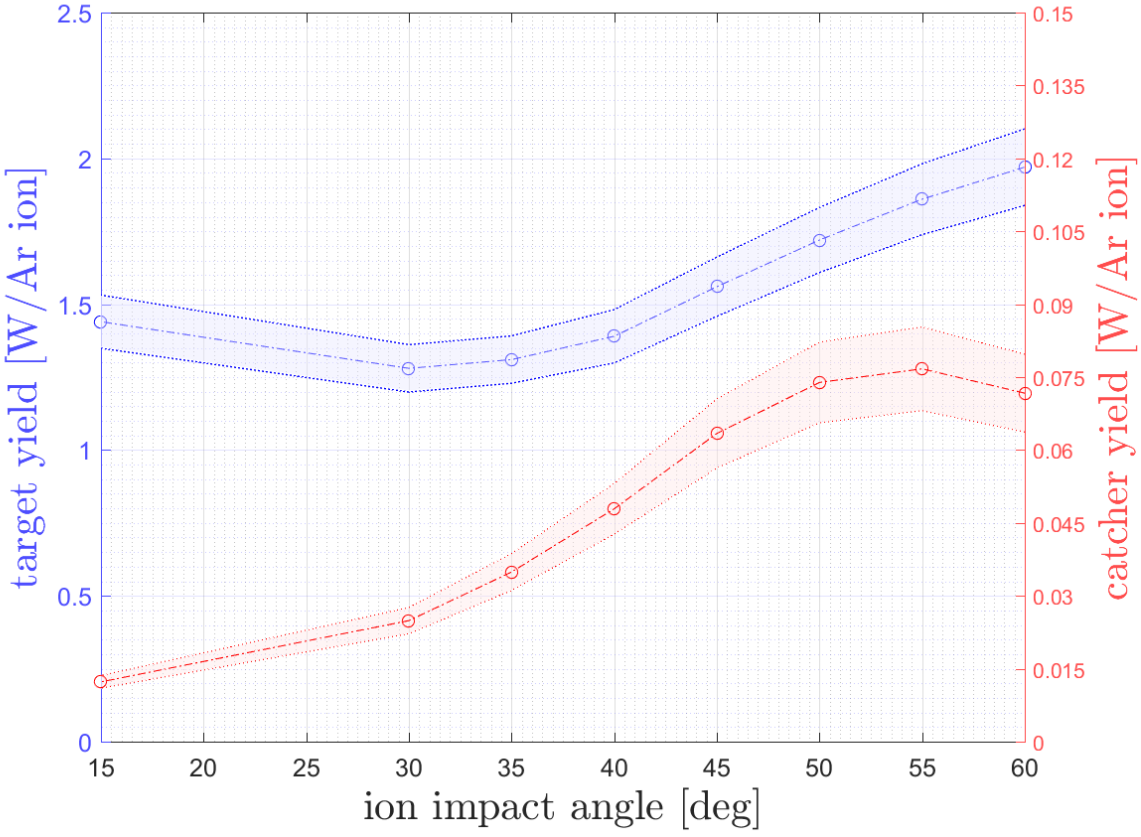

Figure 5.4 – Sputtering yields of a flat W surface as a function of the ion impact angle α with respect to the target's surface normal under 2 keV Ar^{1+} ion bombardment. The catcher parameters were set to: $\Delta x = 1$ mm and $d = 13$ mm. The slightly increased target sputtering yield at 15°,can be attributed to a possible contamination film caused by aeration in the course of sample changing. The colored areas indicate the sputtering yield relative errors.

In the next measurement, the catcher parameter Δx was varied, where positive Δx values mean a shift of the target in the ion beam direction. In contrast to the previous measurements, where the ion beam current I_{FC} was almost constant during the entire measurement series and only had to be measured before and after each measurement, it is now necessary to check the ion beam current after each individual measurement point during this Δx measurement series. As can be seen in figure 5.5, the ion beam current decreases linearly in a good approximation with increasing Δx in the measuring range from $\Delta x = -6$ mm to 10 mm. Based on this knowledge, the ion beam current I_{FC} was only explicitly measured at every fourth measuring point for the subsequent Δx measurements and the ion beam current value for the remaining measuring points was interpolated according to the linear behavior.

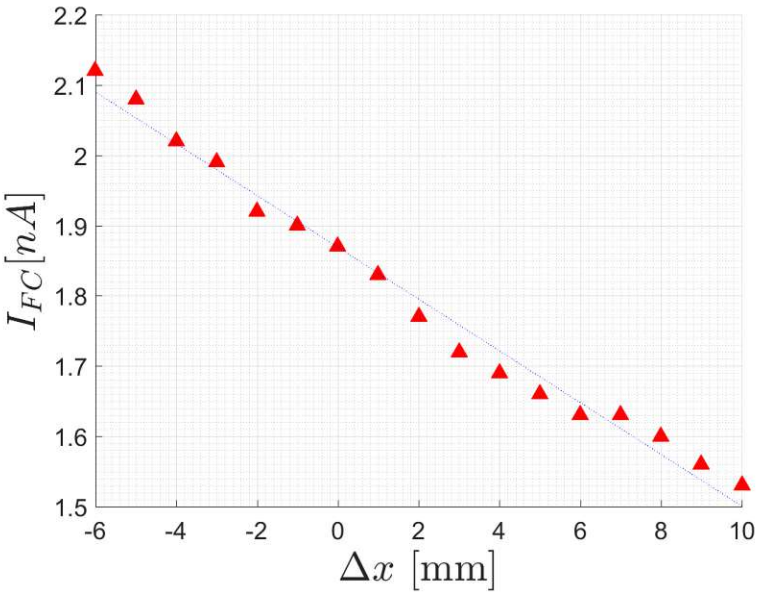

Figure 5.5 – Ion beam current I_{FC} as a function of Δx. By measuring the ion current with the Faraday Cup at the individual measuring points (red triangles), a good approximation of a linear decrease (blue dotted line) of the current with increasing Δx can be seen. Although delta x is defined in relation to the catcher position, it is also a measure of the distance from the ion source to the target holder, which is smallest for $\Delta x = -6$ mm. Over the entire Δx measurement range, an ion current drop of 27% or a percentage current drop of about 1,7% per mm can be observed.

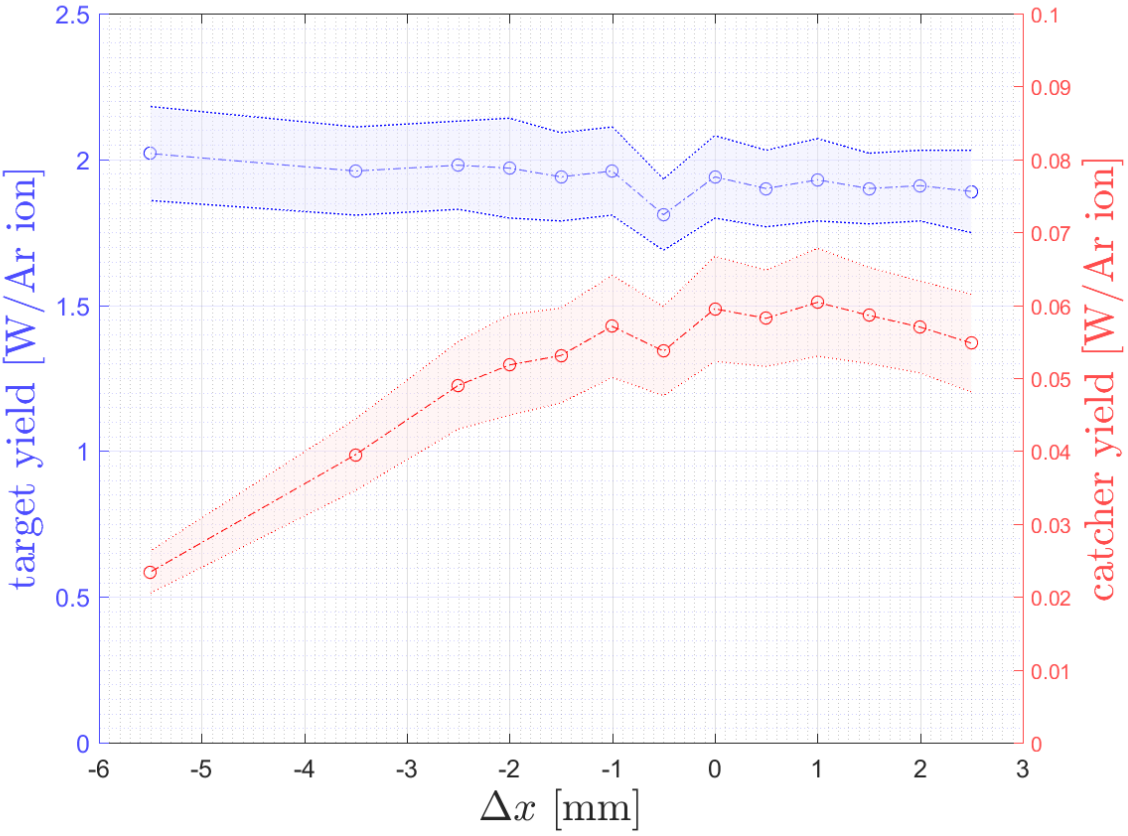

Figure 5.6 – Sputtering yields of a flat W surface as a function of the relative catcher quartz position Δ x along the ion beam direction under 2 keV Ar^{1+} ion bombardment. The catcher parameters were set to: $\alpha = 60°$ and d = 13 mm. Considering the drop of the ion beam current according to figure 5.5 in the evaluation of the sputtering yield, the target yield remains constant. The resulting catcher signal on one hand confirms $\Delta x = 1$ as a good choice as catcher parameter for the other measurements and on the other hand provides important information about the angular distribution of the sputtered particles of the target, illustrated in figure 5.7.

The results of the Δx catcher measurement of the W coated quartz sample are shown in figure 5.6. The angle of incidence of the ion beam was 60° with respect to the surface normal of the target and the catcher distance $d = 13\,\text{mm}$. As only the ion beam current according to figure 5.5 changes for the target, which is taken into account in the evaluation of the erosion rate, the target sputtering yield must of course remain constant. Related to the sputtering distribution, this measurement has the most significant information, since it indirectly provides the angular distribution of the sputtering process via the intensity of the individual catcher signals. In combination with the sputtering simulation program TRI3DYN, R.Stadlmayr et.al. [22, 28] has evaluated this angular distribution for the smooth W coated quartz surface and was able to observe a distinctive sputtering distribution in forward direction, which is illustrated in figure 5.7.

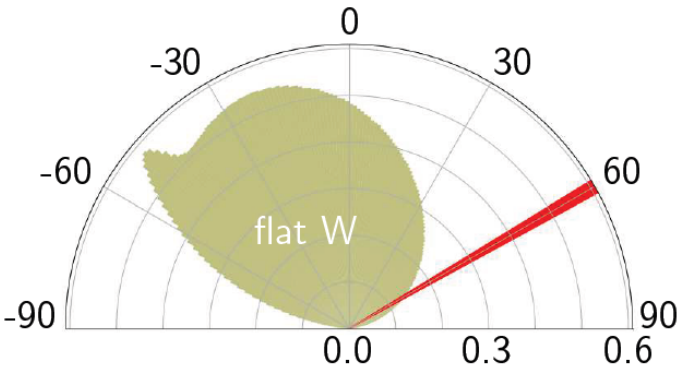

Figure 5.7 – Distribution of sputtered W target particles using a TRI3DYN simulation performed by R.Stadlmayr et.al. The smooth W target surface is hit under an angle of 60° with respect to the surface normal, by an incident 2 keV Ar^{1+} ion beam (red arrow) resulting in a forward directed sputter distribution (colored area) with a single knock-on peak at - 50°. Figure taken from [22, 28].

Another measurement was performed to investigate the dependence of the catcher rate on the distance d as well. Figure 5.8 shows the results of the d - measurement of the W samples. The smallest possible distance between target and catcher is given by $d_{min} = 12.4\,\text{mm}$ and is defined by the zero position of the target holder, where target surface and catcher surface are normal to each other. Even though a catcher measurement at normal ion beam incidence does not make sense, this minimal distance remains, since the target holder must be positioned in the zero position for the individual Faraday Cup current measurements. Since the variation of d does not affect the target sample in any way, the target signal is of course constant again. The expected decrease in the catcher signal is a result of fewer sputtered target particles being able to reach the catcher.

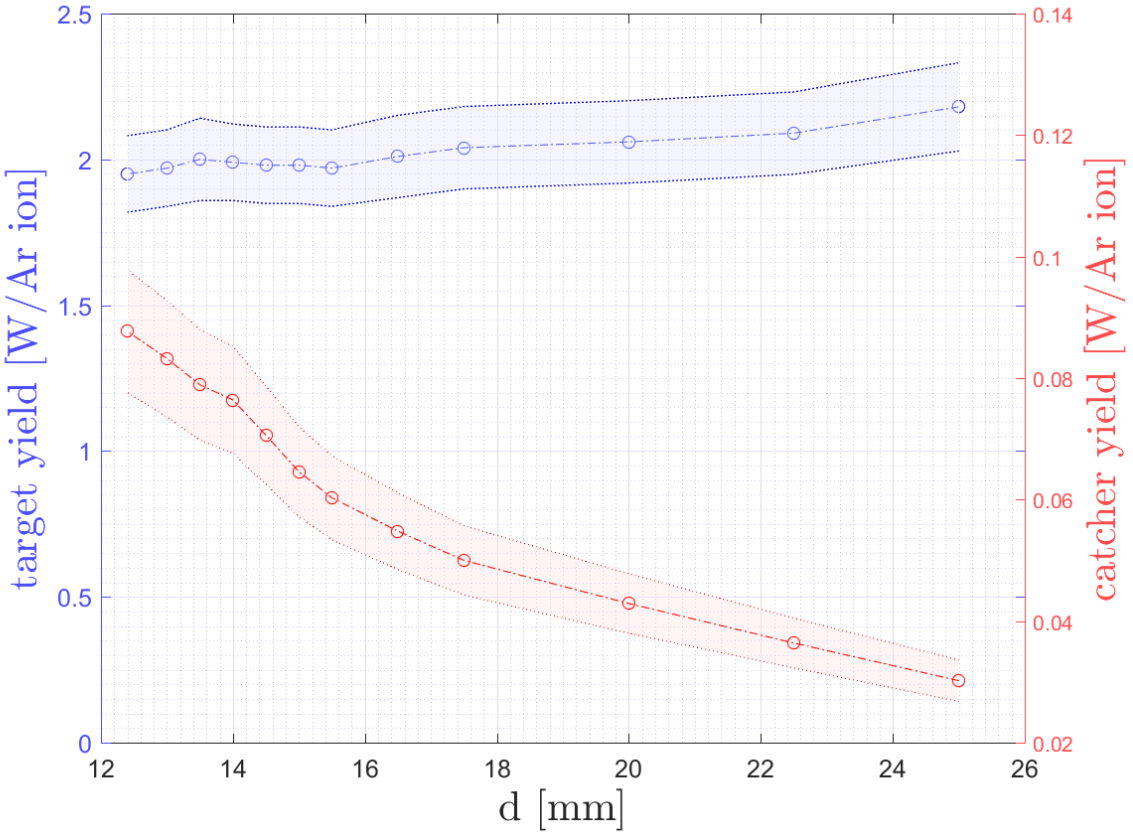

Figure 5.8 – Sputtering yields of a flat W surface as a function of the target-catcher distance d under 2 keV Ar^{1+} ion bombardment. The catcher parameters were set to: $\alpha = 60°$ and $\Delta x = 1$ mm. The closest possible target-catcher distance is given by $d_{min} = 12.4$ mm, since the target holder and the catcher would touch each other if the target holder is in the zero position below this value. The zero position of the target holder is set especially for the FC current measurements. The decrease of the catcher signal can be explained by the fact that less sputtered target particles are able to reach the catcher surface.

With the measurements performed it is now possible to determine the ratio g between catcher yield and target yield for W samples. This information allows to investigate also W bulk samples with the catcher setup and to reconstruct the actual target supttering yield from the measured catcher signal. In figure 5.9 the three evaluations of the g parameter for the W samples are summarized.

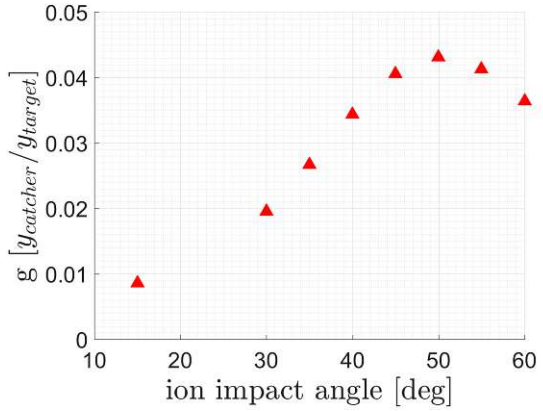

(a) 2 keV $Ar^{1+} \rightarrow W$ ($\Delta x = 1$ mm, $d = 13$ mm)

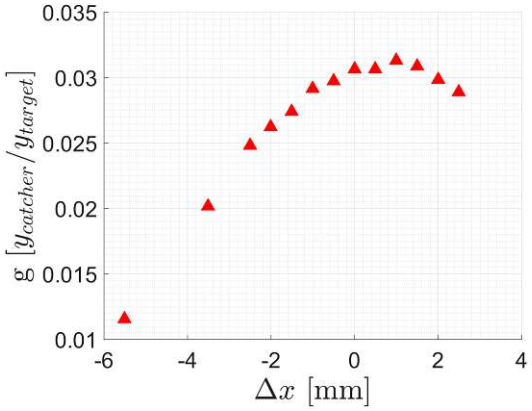

(b) 2 keV $Ar^{1+} \rightarrow W$ ($\alpha = 60°$, $d = 13$ mm)

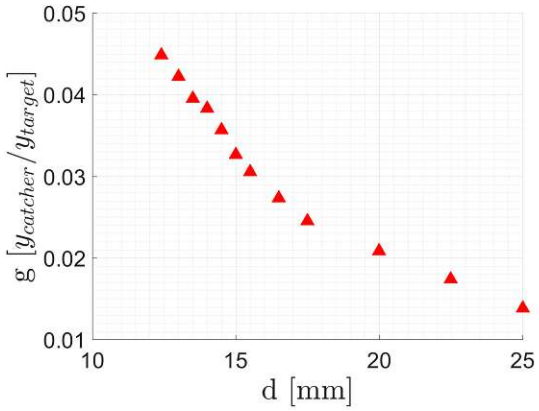

(c) 2 keV $Ar^{1+} \rightarrow W$ ($\alpha = 60°$, $\Delta x = 1$ mm)

Figure 5.9 – Overview of the evaluated g parameters of the W samples, which reveal the ratio of catcher yield and target yield. With these values it is now possible to investigate W bulk samples like W fuzz with the catcher setup and to reconstruct their sputtering yield with its data.

5.3 Ar^{1+} on W Fuzz at 2 keV

As already described in chapter 3.2.1, the surface morphology of tungsten can change fundamentally under certain conditions, all of which may prevail in a future fusion reactor, and forms a microscopic, highly porous surface structure W fuzz [2, 3]. In addition to a significantly reduced thermal conductivity and an almost black body characteristic, it is suspected that this fuzz surface could also have an increased erosion rate due to its composition and thus contaminate the fusion plasma with high-Z impurities to a critical extent [4,5].

Since a W fuzz layer cannot be attached to a conventional quartz crystal due to its complex morphology, the QCM catcher setup is used and the sputtering yield of W Fuzz can be investigated indirectly by catching the sputtered Fuzz particles with a QCM positioned opposite to the fuzz target. The required reference measurements have already been performed in the previous sections 5.1 and 5.2 and it has previously been shown by a test measurement that an ion energy of 500 eV does not provide sufficient frequency changes in the catcher signal, so we had to switch to a higher ion beam energy of 2 keV. SEM images of the W fuzz samples taken by the Forschungszentrum Jühlich (Germany) reveal the amazing, microscopically large and approximately $2\,\mu m$ deep W fuzz structure, shown in figure 5.15. Own analysis efforts with the AFM failed due to the extremely rough surface on the one hand and the black body characteristic on the other hand, as the position and focus finding is acquired via an integrated top-light microscope.

Figure 5.10 – W Fuzz sample inside the target holder.

The W fuzz sample was carefully positioned in the target holder as shown in figure 5.10 and attached to the manipulator in the UHV chamber accordingly. In order to obtain a direct comparison of the catcher signal between W fuzz and the flat W sample, the same smooth W coated quartz crystal was used as catcher quartz as in the previous measurements described in 5.2.

Finally, the W fuzz sample was exposed to a stepwise 2 keV Ar^{1+} ion bombardment and measurements were taken after each applied fluence step. The resulting W fuzz measurements are presented in figure 5.11 in direct comparison with the smooth W target previously studied in section 5.2.

Two things can be clearly seen from the measurement results. First, the W fuzz sample surprisingly exhibits a much lower sputtering yield than the smooth W sample, although the initial measurement of the virgin (apart from the negligible Ar fluence in the course of the Δx measurement) W fuzz sample could may have involved an accumulation of a thin oxide layer on the fuzz surface due to intermediate storage in air, which may additionally dampen the sputtering yield. On the other hand, the distribution of the caught W fuzz particles is much broader, which is due to the extremely rough surface characteristics of the fuzz structure and thus makes a distribution almost over the entire scanned Δx measuring range possible.

Furthermore, an increase in the erosion rate of the sputtering yield with increasing applied Ar ion fluence can be observed. A possible explanation for the behavior of the W fuzz sputtering yield is that incident Ar ions release individual W atoms from the fuzz strings, but these re-attach to neighboring strings, leading to a dynamic change in the fuzz surface, which becomes more and more aligned in the ion beam direction with increasing deposited Ar ion fluence. The increase in erosion can then be explained by the fact that the W fuzz strings become denser with increasing Ar ion fluence according to the ion beam direction, but also shorter and shorter, and accordingly there is less chance that sputtered W fuzz particles can reattach to neighboring fuzz strings.

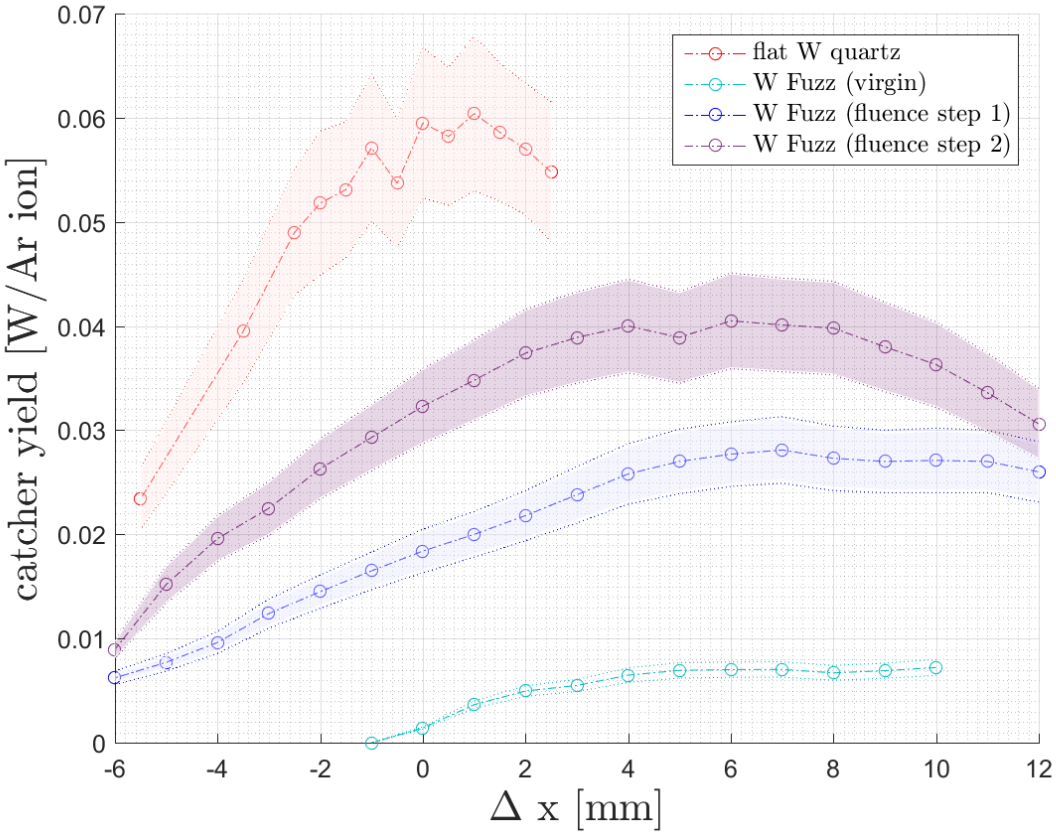

Figure 5.11 – Comparison of catcher measurements between a flat W coated quartz crystal sample (red) and a W fuzz target. The W Fuzz sample was exposed to a stepwise long-term 2 keV Ar^{1+} ion irradiation under 60° with respect to the target's surface normal. The virgin fuzz surface (aqua) exhibits a very low catcheryield, which could be explained by redeposition processes of the rough fuzz surface. After an applied Ar^{1+} ion fluence of $\Phi_1 = 4{,}277 \cdot 10^{20}$ Ar/m² (fluence step 1, blue) the sputtering yield increases throughout the entire Δx measurement spectrum, and after an applied fluence of $\Phi_2 = 8{,}597 \cdot 10^{20}$ Ar/m² (fluence step 2, magenta) a pronounced maximum of the catcher signal at $\Delta x = 6$ mm is formed, which provides an indication of the sputtering distribution of W Fuzz in the backward direction.

Also to be highlighted is the shifted Δx maximum of the catcher signal in the W fuzz sample at $\Delta x = 6\,\text{mm}$. Looking at the given geometrical arrangement of the catcher setup at $\Delta x = 6\,\text{mm}$, shown in figure 5.12, we can see that the target's surface normal points exactly in the direction of the catcher center and thus W fuzz particles are sputtered preferentially in backward direction.

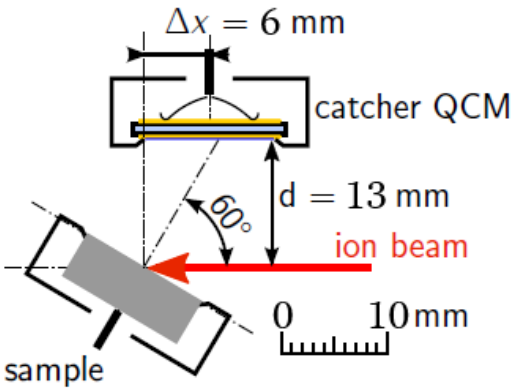

Figure 5.12 – Arrangement of the catcher setup with the W Fuzz sample as target for the shifted maximum $\Delta x = 6\,\text{mm}$. Figure taken and adapted from [22].

A TRI3DYN simulation performed by R.Stadlmayr et.al. [22, 28] illustrates in figure 5.13 the sputtering distribution of the fuzz target and reveals a preferential sputtering in the backward direction.

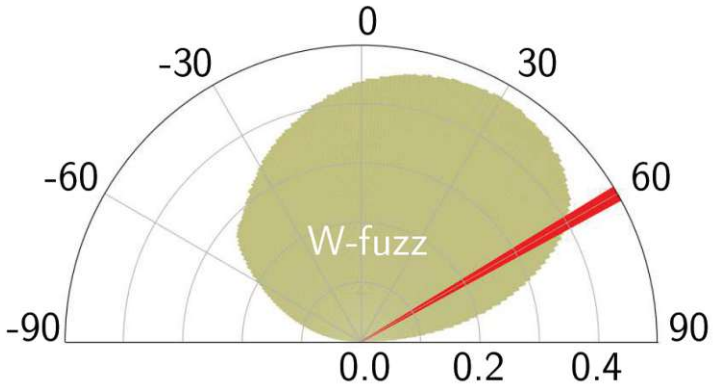

Figure 5.13 – Distribution of sputtered W Fuzz target particles using a TRI3DYN simulation performed by R.Stadlmayr et.al. [22]. The W Fuzz surface is hit under an angle of 60° with respect to the surface normal, by an incident 2 keV Ar^{1+} ion beam (red arrow) resulting in a broad sputter distribution (colored area) with slightly dominant tendency in backward direction. Figure taken from [22, 28]. This is in contrast to the distribution of sputtered W particles from a flat W surface as shown in figure 5.7.

Further experiments with much more intense ion beams even exposed optical changes, which can be seen in figure 5.14. The two impacted regions were exposed to total Ar fluences of $\Phi_{top,spot} = 1{,}76 \cdot 10^{22}$ Ar/m² (top) and $\Phi_{bottom,spot} = 5{,}38 \cdot 10^{21}$ Ar/m² (bottom). Unfortunately, the optical change of the fuzz surface revealed a significant offset of the measurement points, since they should have been oriented centrally along the rotation axis. Closer inspection disclosed a slightly bent manipulator axis, which causes this offset when rotated. This has hardly any effect on the measurements in figure 5.11, since in this case the irradiation was performed with a scanned ion beam, and despite this offset the scanned area can be seen entirely in the center of the W fuzz target. The situation is different with the intensively irradiated measuring points, which were not included in the measurements due to the high error liability.

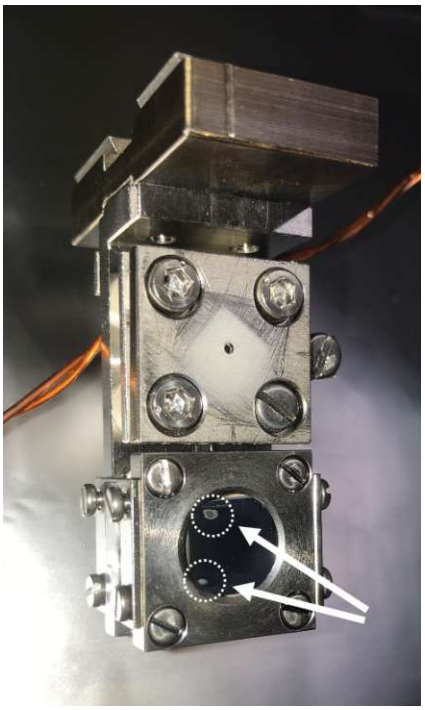

Figure 5.14 – Optical changes of the W fuzz surface caused by intense Ar^{1+} ion irradiation. The applied fluence for the upper measurement point was $\Phi_{top,spot} = 1{,}76 \cdot 10^{22}$ Ar/m² and the applied fluence of the bottom spot was $\Phi_{bottom,spot} = 5{,}38 \cdot 10^{21}$ Ar/m². As an unfortunate secondary finding, a slightly bent manipulator axis was identified, which caused a significant offset of the actual impact points.

Nevertheless, those two intense spots were examined again by SEM, performed by HZDR (Germany) and the impressive results are shown in a general overview 5.15. Figure 5.15(a) and 5.15(b) are still those images of the unirradiated sample. Due to the massive ion irradiation, the entire fuzz structure in the affected area has changed to a scale-like formation. A clear alignment of these scales in the direction of the ion beam, marked by the white arrow can be seen in image 5.15(d). A new FIB cut in image 5.15(f) shows no more fuzz structures even in deeper layers.

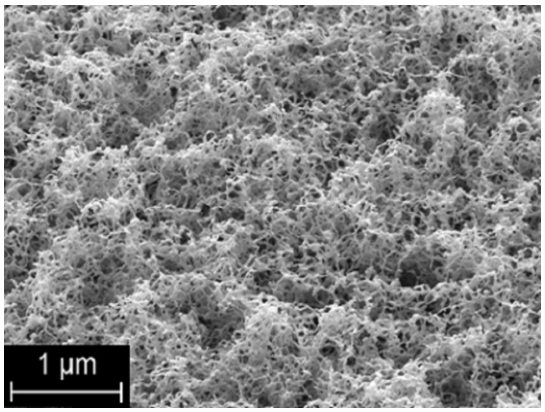

(a) Top view of the virgin W Fuzz layer.

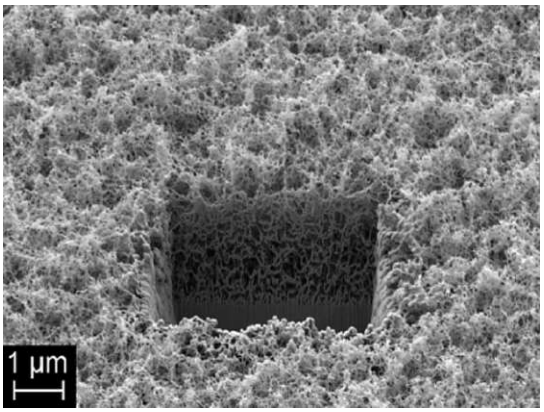

(b) FIB-cut reveals a W Fuzz depth of $2\,\mu m$.

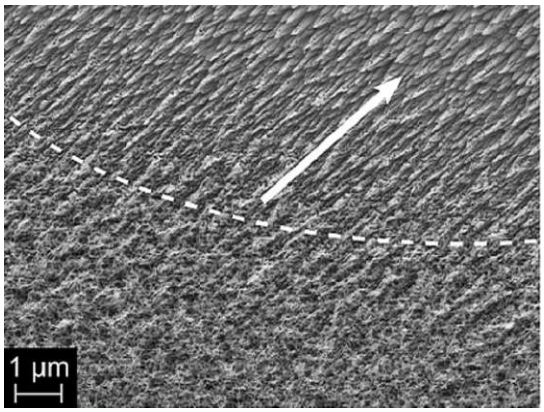

(c) Transition area (white) between irradiated (top) and virgin (bottom) region.

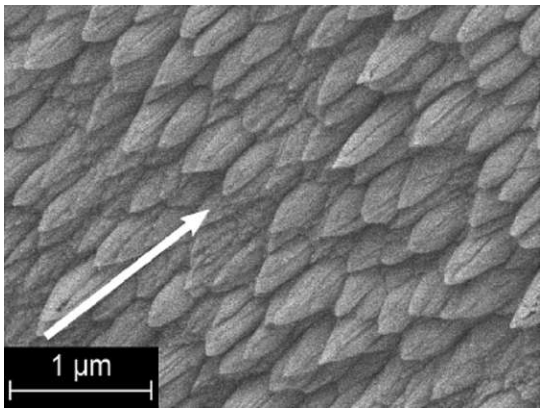

(d) Scaly surface structure of the irradiated region, aligned in ion beam direction (white arrow)

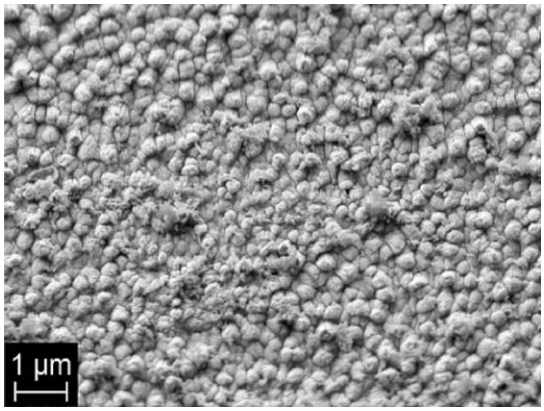

(e) Surface of the irradiated W Fuzz structure as seen from the ion beam perspective

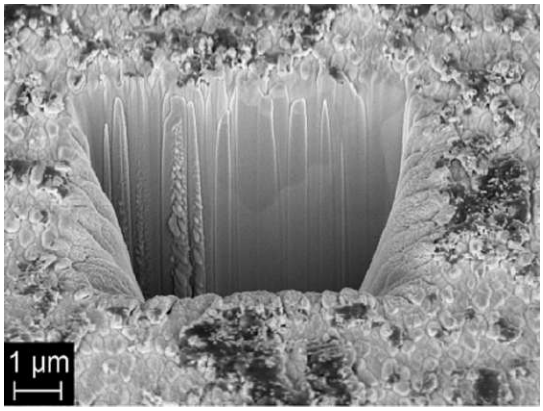

(f) FIB cut of the irradiated sample reveals no residual fuzz structure

Figure 5.15 – SEM images before (a,b) and after (c-f) 2 keV Ar^{1+} ion bombardment under an ion impact angle of 60° with respect to the surface normal. In total an Ar fluence of $\Phi_{tot} = 1{,}76 \cdot 10^{22}$ Ar/m² was applied. SEM analysis was performed by Forschungszentrum Jülich (Germany) and Helmholtz Zentrum Dresden Rossendorf HZDR (Germany). Figures b-f taken from [22, 28].

6 Conclusion

Erosion processes caused by particle bombardment have a significant and very important part in the realization of a future fusion power plant. On the one hand, from an economic point of view, since it is not financially viable to have to replace a complete set of plasma facing components with a new one after only a short period of operation, and on the other hand, from a technical point of view, since especially the eroded high-Z blanket particles can cause the fusion plasma to extinguish even at low amounts. For the divertor area, the most heavily exposed part of the plasma facing materials, tungsten is the material of choice due to its very high melting point, low tritium retention and low sputtering yield [1]. Since it is known that the surface structure of tungsten changes to a highly porous, microscopic W fuzz structure under certain external conditions, which could well be present in a fusion plasma, there is the obvious suspicion that this surface change could exhibit increased erosion behavior [2]. Therefore, the objective of this work was the evaluation of this problem and the investigation of the erosion behavior of W fuzz.

For this purpose, an existing measurement setup was adopted in the AUGUSTIN laboratory of the Institute of Applied Physics at TU Wien and modified according to the new requirements. By using the QCM catcher technique, first smooth W coated quartz crystals and then W fuzz sample were exposed to Ar^{1+} ion bombardment and their corresponding sputteryields were determined by catching the target particles via a catcher QCM. A smooth W coated quartz crystal was also used as catcher quartz in all measurements in order to get the sticking coefficient close to 1. The measurements of the smooth W samples have been necessary to directly compare the catcher yields with the subsequent fuzz measurements on the one hand and on the other hand to determine the important g parameter, which represents the ratio between catcheryield and targetyield and allows a reconstruction of the absolute sputtering yield of the W fuzz sample. Argon was used as working gas, since it will be used as seeding gas in future fusion reactors and is ideally suited due to its noble gas character.

First experiments with an ion energy of 500 eV and an ion incidence angle of 60° with respect to the target's surface normal showed no reaction at all at the catcher signal of the W fuzz sample, in contrast to the smooth W sample. Significant frequency changes could only be seen at the catcher QCM when the kinetic ion energy was 2 keV and above, so a new reference measurement of the smooth samples was performed at 2 keV. These reference measurements made it possible to evaluate the optimal catcher parameters at $\alpha = 50° - 60°$ (ion impact angle with respect to the target's surface normal), $\Delta x = 1$ mm

(offset in ion beam direction) and $d = 13\,\text{mm}$ (distance target to catcher), at which the catcher signal was best. The comparison of the erosion rates clearly shows that W fuzz has a surprisingly much lower sputtering yield than the flat W sample. While the flat W sample has a maximum sputtering yield of $1{,}97 \pm 0{,}13\,\text{W/Ar}$ at an 2 keV Ar^{1+} ion bombardment under an ion impact angle of 60°with respect to the targets normal, the maximum sputtering yield of W Fuzz under same conditions is only 11,6 %, resulting in an absolute sputtering yield of $0{,}23 \pm 0{,}06\,\text{W/Ar}$ when considering the g parameter with the included Δx shift of the W fuzz sample. Applied fluence steps on the W fuzz sample up to a total Ar^{1+} ion fluence of $\Phi_{tot} = 1{,}76 \cdot 10^{22}\,\text{Ar/m}^2$ showed both an increase of the sputtering yield with increasing ion fluence and a significant change of the surface structure, which was clearly visible by SEM images before and after ion irradiation. Based on these SEM images, the low erosion rate of the virgin W fuzz sample can be explained by redeposition, in which already sputtered target particles of the fuzz surface attach to neighboring fuzz strings and thus do not reach the catcher QCM. The ion irradiation leads to a dynamic change of the surface structure aligned in ion beam direction, which gradually changes the complete fuzz morphology into a scale-like surface structure and more and more target particles can leave the target and are captured by the catcher.

In addition, an offset of the maximum sputtering yield in Δx direction could be identified within the W fuzz measurement. A geometrical approach could illustrate that at this Δx shift the surface normal of the target points exactly to the center of the catcher QCM. This means that the sputtered W fuzz particles are preferentially caught in backwards direction by the catcher, while a clear distribution in forward direction was found for the flat W sample. The difference can be explained by the high roughness of the W Fuzz sample.

The measurements for investigating the erosion behavior of W fuzz, which were performed in the course of this research work, do not show an increased erosion rate due to the highly porous surface structure of W fuzz. On the contrary they show a much lower sputtering yield than a smooth, pure W surface and thus represent a promising result for fusion research. However, further measurements are necessary to also investigate the erosion behavior in a relevantly high temperature regime and determine whether the reduction of the thermal conductivity of the W fuzz could affect the sputtering yield.

7 Danksagung

Dieses Kapitel ist mir ein ganz besonderes Anliegen, um meinen unschätzbaren Dank jenen Personen zum Ausdruck zu bringen, die mich über viele Jahre hinweg durch das Studium begleitet haben und ohne deren Unterstützung es wohl nie zu einem Studienabschluss geführt hätte.

Durch die Vorlesung Atomare Stoßprozesse bin ich bereits 2016 im Zuge einer Bachelorarbeit an das Institut für Angewandte Physik gekommen und durfte mich stolz Teil der Arbeitsgruppe Aumayr nennen. Nicht nur die Gruppengröße und Vielfalt (von Bachelorstudentinnen und Bachelorstudenten bis hin zu Dissertantinnen und Dissertanten) haben mich bereits am ersten Tag beeindruckt, sondern vielmehr die unglaublich starke und immer gut gelaunte Team-Moral der gesamten Gruppe. Durch mein wachsendes Interesse an der Fusionsforschung entfaltete sich aus der Bachelorarbeit eine weitere Projektarbeit und kurze Zeit später folgte im Spätherbst 2017 der Start meiner Diplomarbeit. Einem Studienabschluss in Mindestzeit mit Auszeichnung stand eigentlich nichts mehr im Wege...doch es kam leider anders. Die Ausbildung hatte für mich immer einen sehr hohen Stellenwert und ich setzte alles daran stets das Maximum herauszuholen, ganz gleich wie groß die Herausforderung war. Doch am 9. Jänner 2018 wurde ich zum ersten Mal in meinem jungen Leben mit einer Situation konfrontiert, für die es weder Erklärung noch Lösung gibt, dem plötzlichen, komplett unerwarteten Verlustes eines über alles geliebten Familienmitglieds. Leider war dies erst der Beginn eines nicht enden wollenden Albtraums, gefüllt mit unermesslichem Leid, den meine Familie zu ertragen hatte und mich aus meiner bis dato perfekten Welt entriss. Jeder Versuch wieder in die Spur zu finden wurde von einem nächsten, unerwarteten Schicksalsschlag zunichte gemacht und das über mehr als eineinhalb Jahre hinweg andauernd. Das Studium wurde zur absoluten Nebensache, die Motivation dazu fast gänzlich erloschen und selbst der enge Kontakt zur Arbeitsgruppe wurde zunehmend weniger. Nur eine Person ließ über den gesamten, verstrichenen Zeitraum bei der Fertigstellung der Diplomarbeit nie locker!

Lieber Fritz, ich bin mir weder sicher ob es mir auch nur ansatzweise gelingen mag, meinen Dank Dir gegenüber in Worte zu fassen, noch wo ich damit beginnen soll. Es ist einfach nur vorbildhaft, mit welcher Ruhe und Professionalität Du das Institut leitest, wie viel Freude und Hilfsbereitschaft Du für die Arbeitsgruppe ausstrahlst und wie Du zwischen all diesen Tätigkeiten, Vorlesungen und Konferenzen immer irgendwie Zeit findest, um selbst bei Problemen abseits der Lehre zu helfen. Ich hatte im Dezember 2018 meine letzte fehlende Prüfung des Master-Studiums abgelegt und dennoch hätte ich das Studium wohl nie abgeschlossen, wenn Du nicht so hartnäckig geblieben wärst und nicht regelmäßig nachgefragt hättest, wie denn der aktuelle Stand meiner Diplomarbeit aussieht. Und dafür danke ich Dir wirklich von Herzen. Deine Geduld, Gutmütigkeit und Hilfsbereitschaft kennen scheinbar keine Grenzen und zeichnen Dich als besonderen Menschen aus.

Auch bei Dir, lieber Reinhard möchte ich mich für die gemeinsame Forschungszeit bedanken. Du warst nicht nur der Betreuer meiner ersten Projektarbeit am IAP sondern ich durfte dich auch im Zuge deiner Dissertation als Diplomand bei den Messungen unterstützen. Dein Humor, deine Ruhe sowie dein technikaffiner Sinn für Spielereien lassen dich selbst an weniger guten Tagen - Stichwort "Belüftung", "Stromausfall", "Filament gerissen" - nicht im Stich und Du wusstest stets für jedes technische Problem eine praktische Lösung. Es tut mir leid, dass sich mein schriftlicher Teil der Diplomarbeit so derart lange verzögert hat und ich wünsche Dir und deiner jungen Familie alles erdenklich Gute.

Des Weiteren will ich mich ganz herzlich bei meinen lieben Bürokollegen Anna N. und Herbert B. bedanken. Mit euch war es einfach immer lustig, selbst wenn es im Labor mal wieder nicht ganz rund gelaufen ist und ich bereue es, damals nicht schon viel früher aus "meinem" AFM Kammerl herunter gekommen zu sein. Gemeinsam haben wir versucht Herbert's Elektronirätsel zu lösen, haben gemeinsam die spektakuläre Softskill-Vorlesung "Technik für Menschen" bestritten und haben uns bei Gelegenheit gegenseitig kleine Streiche im Büro gespielt.
Anna, für Dich scheint wirklich keine Herausforderung zu groß zu sein. Du engagierst Dich gefühlt 24h/Tag für die Arbeitsgruppe und hilfst einfach überall, sei es im Labor, beim Lernen für Prüfungen oder bei der Organisation von AG Ausflügen. Ich bin mir sicher, dass Du auch deine Doktorarbeit mit Bravur meistern und deine Ausbildung verdient mit dem Ring der Macht abschließen wirst (P.S. Um welchen Film könnte es sich handeln?).
Herbert, mit deinem Salzburger Schmäh verbeitest Du jederorts positive Stimmung und Dein praxisbezogenes Technikverständnis, speziell in der Elektronik sind bewundernswert. Aber auch abseits der Uni bist Du auf der Erfolgsspur, hast uns an deinem Glück bei Deiner Traumhochzeit teilhaben lassen und stehst mit Deiner eigenen Familie bereits fest im Leben.

Ein weitere Dank gilt Christian C. und Paul S., die mich durch eine zweite Projektarbeit während meiner kritischen Phase wieder zurück ans Institut brachten und mir dadurch geholfen haben, einen neuerlichen Anschluss zur Arbeitsgruppe zu finden. Dies hat wesentlich dazu beigetragen, meine Diplomarbeit fortzuführen und in weiterer Folge sogar abzuschließen.

Auch bei den restlichen, zahlreichen Kolleginnen und Kollegen der Arbeitsgruppe Elisabeth G., Florian L., Bernhard B., Lorenz B., Janine S., David M., Georg H., Richard W., Gabriel S., Johanna F., Lidija R., Bernd S. möchte ich mich für die wunderbare gemeinsame Zeit in der Arbeitsgruppe AU bedanken und wünsche allen viel Erfolg und alles Glück der Welt für den weiteren Lebensweg.

Zu guter Letzt möchte ich mich bei meiner gesamten Familie bedanken, die eine mehr als nur schwierige und vor allem mit Trauer erfüllte Zeit hinter sich hat. Es bedeutet mir unendlich viel selbst unter solchen Umständen jederzeit einen sicheren Rückhalt zu haben, auch wenn der Abschluss meiner Diplomarbeit mehrmals für Spannungen und Verzweiflung gesorgt hat.

„Erfolg besteht darin, dass man genau die Fähigkeiten hat, die im Moment gefragt sind.“ - Henry Ford [45]

Bibliography

[1] J.W.Coenen, M.Berger, M.J.Demkowicz, D.Matveev, A.Manhard, R.Neu, J.Riesch, B.Unterberg, M.Wirtz, and Ch.Linsmeier. Plasma-wall interaction of advanced materials. *Nuclear Materials and Energy*, 12:307–312, 2017.

[2] H. Iwakiri, K. Yasunaga, K. Morishita, and N. Yoshida. Microstructure evolution in tungsten during low-energy helium ion irradiation. *Journal of Nuclear Materials*, 283-287:1134–1138, 2000.

[3] D. Nishijima, M.Y. Ye, N. Ohno, and S. Takamura. Incident ion energy dependence of bubble formation on tungsten surface with low energy and high flux helium plasma. *Journal of Nuclear Materials*, 313-316:97–101, 2003.

[4] S. Kajita, S. Takamura, N. Ohno, D. Nishijima, H. Iwakiri, and N. Yoshida. Sub-ms laser pulse irradiation on tungsten target damaged by exposure to helium plasma. *Nuclear Fusion*, 47:1358–1366, 2007.

[5] W. Sakaguchi, S. Kajita, N. Ohno, and M. Takagi. In situ reflectivity of tungsten mirrors under he plasma exposure. *Journal of Nuclear Materials*, 390-391:1149–1152, 2009.

[6] IEA. world total energy supply by source (2018). `https://www.iea.org/reports/key-world-energy-statistics-2020`.

[7] Hannah Ritchie and Max Roser. Global energy consumption. *Our World in Data*, 2020. `https://ourworldindata.org/energy-production-consumption`.

[8] IRENA. Trends in renewable energy. `https://www.irena.org/Statistics/View-Data-by-Topic/Capacity-and-Generation/Statistics-Time-Series`.

[9] statista. Mortality rate worlwide in 2012 by energy source. `https://www.statista.com/statistics/494425/death-rate-worldwide-by-energy-source/`.

[10] Hannah Ritchie and Max Roser. Death rates from energy production per Twh. *Our World in Data*, 2020. `https://ourworldindata.org/nuclear-energy?country=#what-are-the-safest-sources-of-energy`.

[11] J. Raeder, A. Weller, R. Wolf, X. Jin, L. Boccaccini, R. Stieglitz, D. Carloni, C. Pistner, and J. Herb. Review of the safety concept for fusion reactor concepts and transferability of the nuclear fission regulation to potential fusion power plants. Technical report, Gesellschaft fuer Anlagen- und Reaktorsicherheit mbH (GRS), 2016.

[12] W. Gebhardt. Skriptum Nukleare Astrophysik. `http://www.physik.uni-regensburg.de/forschung/gebhardt/gebhardt_files/skripten/Kernreaktionen.pdf`.

[13] W. Demtröder. *Experimentalphysik 4*. Springer Spektrum, 2013. (Seiten 310-312).

[14] Kamelander G. Grundlagen der Plasmatheorie mit besonderer Berücksichtigung der Fusionsphysik. Lecture notes.

[15] H.S. Bosch and G.M. Hale. Improved formulas for fusion cross-sections and thermal reactivities. *Nuclear Fusion*, 32:611, 1992.

[16] T. Oesterreicher. Alternative Nukleare Energiesysteme. Lecture notes. p.55.

[17] ITER Organisation, 2021. `https://www.iter.org/`.

[18] Janeschitz G. Plasma-wall interaction issues in iter. *Journal of Nuclear Materials*, 1:290–293, 2001.

[19] R.A. Pitts, A. Kukushkin, A. Loarte, A. Martin, M. Merola, C.E. Kessel, V. Komarov, and M. Shimada. Status and physics basis of the ITER divertor. *Physica Scripta*, 2009.

[20] S. Putvinski, L. Baylor, D. Campbell, V. Chuyanov, Y. Gribov, V. Leonov, A. Loarte, S. Maruyama, R. Pearce, R.A. Pitts, A. Polevoi, R. Mitteau, and M. Sugihara. Disruption mitigation in ITER. ITER Publications. `https://www-pub.iaea.org/mtcd/meetings/PDFplus/2010/cn180/cn180_papers/itr_1-6.pdf`.

[21] U. Kruezi, S. Jachmich, H.S. Koslowski, M. Lehnen, S. Brezinsek, G. Matthews, and JET EFDA Contributors. A new Disruption Mitigation System for deuterium-tritium operation at JET. *Fusion Engineering and Design*, 96-96:286–289, 2015.

[22] R. Stadlmayr, P.S. Szabo, D. Mayer, T. Cupak, C.and Dittmar, L. Bischoff, S. Möller, Rasinski M., R.A. Wilhelm, W. Möller, and F. Aumayr. Sputtering of nanustructured tungsten and comparison to modelling wit TRI3DYN. *Journal of Nuclear Materials*, 532, 2020.

[23] R. Behrisch and W. Eckstein. *Sputtering by Particle Bombardment*. Springer, 2007.

[24] R.A. Wilhelm. Ion-Solid Interaction. Lecture notes, 2018.

[25] R. Arredondo, M. Oberkofler, T. Schwarz-Selinger, U. von Toussaint, V.V. Burwitz, A. Mutzke, E. Vassallo, and M. Pedroni. Angle-dependent sputter yield measurements of keV D ions on W and Fe and comparison with SDTrimSP and SDTrimSP-3D. *Nuclear Materials and Energy*, 18:72, 2019.

[26] R. Stadlmayr, P.S. Szabo, D. Mayer, C. Cupak, W. Möller, and F. Aumayr. Erosion of iron-tungsten model films by deuterium ion irradiation: a benchmark for TRI3DYN. *Physica Scripta*, T171, 2020.

[27] R. Stadlmayr, P.S. Szabo, B.M. Berger, R. Cupak, C.and Chiba, D. Blöch, D. Mayer, B. Stechauner, M. Sauer, A. Foelske-Schmitz, M. Oberkofler, T. Schwarz-Selinger, A. Mutzke, and F. Aumayr. Fluence dependent changes of surface morphology and sputtering yield of iron: Comparison of experiments with SDTrimSP-2D. *Nuclear Instruments and Methods in Physics Research Section B: Beam Interactions with Materials and Atoms*, 430:42–46, 2018.

[28] R. Stadlmayr. *Erosion of Fusion Relevant Materials-Experiments and Modelling*. PhD thesis, TU Wien, 2020.

[29] G. Sauerbrey. Verwendung von Schwingquarzen zur Wägung dünner Schichten und zur Mikrowägung. *Zeitschrift für Physik*, 155:206, 1959.

[30] G. Hayderer, M. Schmid, P. Varga, HP. Winter, and F. Aumayr. A highly sensitive quartz-crystal microbalance for sputtering investigations in slow ion-surface collisions. *Review of Scientific Instruments*, 1999.

[31] R. Stadlmayr, P.S. Szabo, H. Biber, H.R. Koslowski, E. Kadletz, C. Cupak, R.A. Wilhelm, M. Schmid, C. Linsmeier, and F. Aumayr. A high temperature dual-mode quartz crystal microbalance technique for erosion and thermal desorption spectroscopy measurements. *Review of Scientific Instruments*, 91, 2020.

[32] A. Golczewski, K. Dobes, G. Wachter, M. Schmid, and F. Aumayr. A quartz-crystal-microbalance technique to investigate ion-induced erosion of fusion relevant surfaces. *Nuclear Instruments and Methods in Physics Research Section B: Beam Interactions with Materials and Atoms*, 267:695–699, 2009.

[33] B.M. Berger. *Laboratory work on plasma-wall-interaction prprocess relevant for fusion experiments*. PhD thesis, TU Wien, 2017.

[34] P.S.Szabo. Experimental and simulated sputtering of gold, iron and wollastonite with a catcher-qcm setup. Master's thesis, TU Wien, 2017.

[35] B.M.Berger, P.S.Szabo, R.Stadlmayr, and F.Aumayr. Sputtering measurements using a quartz crystal microbalance as a catcher. *Nuclear Instruments and Methods in Physics Research Section B: Beam Interactions with Materials and Atoms*, 2016.

[36] W. Auzinger, C. Schmeiser, and E. Weinmüller. Praktische Mathematik II für TPH. Lecture notes, 2012. p.45.

[37] The MathWorks inc. `https://de.mathworks.com/help/matlab/ref/conv.html`.

[38] M. Schmid. *Möglichkeiten und Grenzen der Schwingquarz-Schichtdickenmessung*. PhD thesis, TU Wien, 1989.

[39] R. Stadlmayr. Erosion of tungsten-nitride and iron-tungsten surfaces under deuterium ion impact. Master's thesis, TU Wien, 2016.

[40] S. Brezinsek, J.W. Coenen, T. Schwarz-Selinger, K. Schmid, A. Kirschner, A. Hakola, F.L. Tabares, H.J. van der Meiden, M.-L. Mayoral, M. Reinhart, E. Tsitrone, T. Ahlgren, M. Aints, M. Airila, S. Almaviva, E. Alves, T. Angot, V. Anita, R. Arredondo Parra, F. Aumayr, M. Balden, J. Bauer, M. Ben Yaala, B.M. Berger, R. Bisson, C. Björkas, I. Bogdanovic Radovic, D. Borodin, J. Bucalossi, J. Butikova, B. Butoi, I. Čadež, R. Caniello, L. Caneve, G. Cartry, N. Catarino, M. Čekada, G. Ciraolo, L. Ciupinski, F. Colao, Y. Corre, C. Costin, T. Craciunescu, A. Cremona, M. De Angeli, A. de Castro, R. Dejarnac, D. Dellasega, P. Dinca, T. Dittmar, C. Dobrea, P. Hansen, A. Drenik, T. Eich, S. Elgeti, D. Falie, N. Fedorczak, Y. Ferro, T. Fornal, E. Fortuna-Zalesna, L. Gao, P. Gasior, M. Gherendi, F. Ghezzi, Ž. Gosar, H. Greuner, E. Grigore, C. Grisolia, M. Groth, M. Gruca, J. Grzonka, J.P. Gunn, K. Hassouni, K. Heinola, T. Höschen, S. Huber, W. Jacob, I. Jepu, X. Jiang, I. Jogi, A. Kaiser, J. Karhunen, M. Kelemen, M. Köppen, H.R. Koslowski, A. Kreter, M. Kubkowska, M. Laan, L. Laguardia, A. Lahtinen, A. Lasa, V. Lazic, N. Lemahieu, J. Likonen, J. Linke, A. Litnovsky, Ch. Linsmeier, T. Loewenhoff, C. Lungu, M. Lungu, G. Maddaluno, H. Maier, T. Makkonen, A. Manhard, Y. Marandet, S. Markelj, L. Marot, C. Martin, A.B. Martin-Rojo, Y. Martynova, R. Mateus, D. Matveev, M. Mayer, G. Meisl, N. Mellet, A. Michau, J. Miettunen, S. Möller, T.W. Morgan, J. Mougenot, M. Mozetič, V. Nemanič, R. Neu, K. Nordlund, M. Oberkofler, E. Oyarzabal, M. Panjan, C. Pardanaud, P. Paris, M. Passoni, B. Pegourie, P. Pelicon, P. Petersson, K. Piip, G. Pintsuk, G.O. Pompilian, G. Popa, C. Porosnicu, G. Primc, M. Probst, J. Räisänen, M. Rasinski, S. Ratynskaia, D. Reiser, D. Ricci, M. Richou, J. Riesch, G. Riva, M. Rosinski, P. Roubin, M. Rubel, C. Ruset, E. Safi, G. Sergienko, Z. Siketic, A. Sima, B. Spilker, R. Stadlmayr, I. Steudel, P. Ström, T. Tadic, D. Tafalla, I. Tale, D. Terentyev, A. Terra, V. Tiron, I. Tiseanu, P. Tolias, D. Tskhakaya, A. Uccello, B. Unterberg, I. Uytdenhoven, E. Vassallo, P. Vavpetič, P. Veis, I.L. Velicu, J.W.M. Vernimmen, A. Voitkans, U. von Toussaint, A. Weckmann, M. Wirtz, A. Založnik, and R. Zaplotnik. Plasma–wall interaction studies within the EUROfusion consortium: progress on plasma-facing components development and qualification. *Nuclear Fusion*, 57(11):116041, aug 2017.

[41] M.Oberkofler, D.Alegre, F.Aumayr, S.Brezinsek, T.Dittmar, K.Dobes, D.Douai, A.Drenik, M.Köppen, U.Kruezi, Ch.Linsmeier, C.P.Lungu, G.Meisl, M.Mozetic, C.Porosnicu, V.Rohde, S.G.Romanelli, the ASDEX Upgrade Team, and JET EFDA Contributors. Plasma-wall interaction with nitrogen seeding in all-metal fusion devices: Formation of nitrides and ammonia. *Fusion Engineering and Design*, pages 1371–1374, 2015.

[42] K.Ikuse, S.Yoshimura, M.Kiuchi, K.Hine, and S.Hamaguchi. Measurement of sticking probability and sputtering yield of au by low-energy mass selected ion beams with a quartz crystal microbalance. *Journal of Physics: Conference Series*, 106, 2008.

[43] S. Kajita, N. Sakaguchi, W.and Ohno, N. Yoshida, and T. Saeki. Formation process of tungsten nanustructure by the exposure to helium exposure under fusion relevant plasma conditions. *Nuclear Fusion*, 49, 2009.

[44] D. Nishijima, M.J. Baldwin, R.P. Doemer, and J.H. Yu. Sputtering properties of tungsten 'fuzzy' surfaces. *Journal of Nuclear Materials*, 415:96–99, 2011.

[45] `https://www.zitate.eu/autor/henry-ford-zitate/28421`.